CTF SYSTEMS INC.

CA1
DTC 800
89
F17

TP9779E

CA1
DTC800-
89
F17

421417

41.D

Fabrication and Testing of a Superconducting Coil Phase 3 of the Maglev Development Program

Prepared for the
Transportation Development Centre
Policy and Coordination Group
Transport Canada

by

A. A. Fife, S. Lee, M. Tillotson

CTF Systems Inc.

Library and Information Centre / Transport Canada / Transports Canada
JAN 9 1990

March, 1989.

421417

DISCLAIMER

The contents of this report reflect the views of CTF Systems Inc., and not necessarily the official view or opinions of the Transportation Development Centre of Transport Canada.

LANGUAGE NOTICE

Un sommaire en français de ce rapport est inclus avant la table des matières.

Project Team (CTF Systems Inc. Staff).

Name	CTF Title	Function
A. A. Fife	Senior R & D Manager	Project Leader
M.B. Burbank	President	Financial Management
J. Vrba	Vice-President	Project Mangement
S. Lee	Physicist	System Design, Experimental Testing and Analysis
K. Betts	Electrical Engineer	System Design and Testing
M. Tillotson	R & D Technical Specialist	System Design, Experimental Testing
W. Westera	Production Manager	System Production
M. Szegedi	Machinist	System Fabrication
S. Parker	Electronics Technician	Electrical System Fabrication
J. Gartner	Draftsperson	General System Drafting
J. Nomura	R &D Technician	General Technical Work
B. Andrews	Mechanical Technician	General Technical Work
R. Westera	Mechanical Technician	General Technical Work

Transport Canada / Transports Canada

PUBLICATION DATA FORM

1. Transport Canada Publication No.	2. Project No.	3. Recipient's Catalogue No.
TP9779E	6675	

4. Title and Subtitle

FABRICATION AND TESTING OF A SUPERCONDUCTING COIL PHASE 3 OF THE MAGLEV DEVELOPMENT PROGRAM

5. Publication Date

March, 1989

6. Performing Organization Document No.

7. Author(s)

A.A. Fife

8. Transport Canada File No.

D1465-475-1

9. Performing Organization Name and Address

CTF Systems Inc.
15-1750 McLean Avenue
Port Coquitlam, B.C.
V3C 1M9

10. DSS File No.

T8200-6-6501

11. DSS or Transport Canada Contract No.

T8200-6-6501/01-SB

12. Sponsoring Agency Name and Address

Transportation Development Center (TDC)
Guy Favreau Complex
200 René Lévesque Blvd. West
West Tower, Suite 601
Montreal, Quebec H2Z-1X4

13. Type of Publication and Period Covered

Final

14. Project Officer

M. Audette

15. Supplementary Notes (Funding programs, titles of related publications, etc.)

16. Abstract This report documents developmental research on superconducting magnet technology suitable for the levitation and propulsion units of the Canadian Maglev vehicle. The contract work involved the design, fabrication and testing of a racetrack coil fabricated using epoxy-impregnated windings of copper stabilized NbTi wire. The following results were achieved:

- successful fabrication and testing of a superconducting racetrack magnet with strength > 400,000 A-turns integrated in a support frame;
- selection and characterization of cryogenic strain gauges;
- characterization of strain in solenoidal and racetrack superconducting magnets;
- design, fabrication and testing of high current persistent switches;
- operation of superconducting magnets in persistent mode.

The racetrack coil reached the design current after the third quench and short sample critical current after the eighth quench. This behaviour is essentially identical to that observed with a superconducting solenoid fabricated during a previous phase of the Maglev activity at CTF. The strain measured perpendicular to the straight sides of the racetrack coil was proportional to the square of the energizing current.

Persistent switches were fabricated - one type with low resistance (10^{-2} ohm) and the other with high resistance (1.2 ohm) in their normal states. The low resistance switch could be operated with stable characteristics up to about 800A drive current (in ≈ 1 Tesla field) and the high resistance switch to 475A (also in ≈ 1 Tesla).

17. Key Words

Magnetic levitation, suspension, superconducting magnet, epoxy-impregnated copper stabilized, niobium titanium coil

18. Distribution Statement

Limited number of copies available from the Transportation Development Centre

19. Security Classification (of this publication)	20. Security Classification (of this page)	21. Declassification (date)	22. No. of Pages	23. Price
N/A	N/A			

Transports Canada Transport Canada

FORMULE DE DONNÉES POUR PUBLICATION

1. N° de la publication de Transports Canada	2. N° de l'étude	3. N° de catalogue du destinataire
TP 9779E	6675	

4. Titre et sous-titre	5. Date de la publication
FABRICATION AND TESTING OF A UPERCONDUCTING COIL PHASE 3 OF THE MAGLEV DEVELOPMENT PROGRAM	Mars, 1989
	6. N° du document de l'organisme exécutant
7. Auteur(s)	8. N° de dossier — Transports Canada
A.A. Fife	D1465-475-1
9. Nom et adresse de l'organisme exécutant CTF Systems Inc. 15-1750 McLean Avenue Port Coquitlam C.B. V3C 1M9	10 N° de dossier — ASC T8200-6-6501
	11. N° de contrat — ASC ou Transports Canada T8200-6-6501/01-SB
12. Nom et adresse de l'organisme parrain Centre de développement des transports (CDT) 200 ouest, boul. René-Lévesque Suite 601, tour ouest Montréal (Québec) H2Z 1X4	13. Genre de publication et période visée Final
	14. Agent de projet M. Audette

15. Remarques additionnelles (Programmes de financement, titres de publications connexes, etc.)

16. Résumé Le présent rapport fait état des recherches de développement concernant des aimants supraconducteurs pouvant servir à assurer la sustentation et la propulsion du Maglev canadien. Les travaux comprenaient la conception, la fabrication et l'essai d'une bobine ovalisée faite d'enroulements de fil de NbTi stabilisé au cuivre et imprégné de résine époxydique. Voici les résultats obtenus: -fabrication et essais concluants d'un aimant ovalisé supraconducteur d'une résistance de 400 000> A/tr monté dans un cadre; choix et caractérisation des extensomètres cryogènes; caractérisation des contraintes dans les aimants supraconducteurs cylindriques et ovalisés; conception, fabrication et essai d'interrupteurs persistants à courant élevé; fonctionnement des aimants supraconducteurs en mode persistant.

La bobine ovalisée a atteint le courant nominal de fonctionnement après la troisième transition, et le courant critique, mesuré sur de petits échantillons, après la huitième transition, situation essentiellement identique aux résultats observés sur une bobine cylindrique supraconductrice fabriquée lors d'une étape précédente dans le cadre du projet Maglev chez CTF. La déformation mesurée normalement aux côtés droits de la bobine ovalisée était proportionnelle au carré du courant d'excitation.

Fabrication de deux types d'interrupteurs persistants: il s'agit d'un interrupteur à faible résistance et d'un interrupteur à résistance élevée, à l'état normal. L'interrupteur à faible résistance pouvait être activé sans aucun changement de ses caractéristiques jusqu'à un courant nominal de 800 A (dans un champ d'environ 1 tesla) tandis que l'interrupteur à résistance élevée ne pouvait pas dépasser 475 A (également environ 1 tesla).

17. Mots clés	18. Diffusion
Sustentation magnétique. Suspension. Aimant supraconducteur. Résine époxydique. Bobine de niobium et titanium.	Le Centre de développement des transports dispose d'un nombre limité d'exemplaires.

19. Classification de sécurité (de cette publication)	20. Classification de sécurité (de cette page)	21. Déclassification (date)	22. Nombre de pages	23. Prix
non classsifiée	non classifiée			

CDT/TDC 79-005 Rev 88

Canada

SUMMARY

This report documents a research and development contract entitled: "Fabrication and Testing of a Superconducting Coil - Phase 3 of the Maglev Development Program". The work was sponsored by the Transportation Development Centre of Transport Canada (TDC), and carried out by CTF Systems Inc. of Port Coquitlam, B.C (CTF).

This research is related to the Canadian Maglev program, which has been a long-range R & D effort aimed at the deployment of non-contact transportation technology in selected Canadian traffic corridors. It has been recognized that it may be several decades before it is economically feasible to deploy such a system within the Canadian context. As a result, it has been decided to adopt the strategy of maintaining a relatively modest level of R & D in Maglev in order to develop and maintain the expertise within Canada necessary to exploit Maglev when the need becomes apparent, and also in the expectation of near-term economic benefits to transportation and other emerging technologies.

In this particular contract, the focus has been on the industrial development of superconducting magnet technology which includes superconducting racetrack coils and persistent mode switches operating at 4.2 K temperature. This extends the work on solenoidal (circular) coils which was reported in "Fabrication and Testing of Reduced-Scale Superconducting Magnets" Transport Canada Report No. TP7949E, prepared by CTF Systems, July, 1986.

The objective of the contract project was to: "Fabricate, test and evaluate a fully instrumented superconducting coil with racetrack geometry utilizing epoxy impregnation techniques developed in prior work". During the contract, the remarkable discovery of high temperature (High Tc) superconductors took place, and it was decided to amend the contract to include some work on the High Tc materials. The amendment was granted after the successful development of an instrumented half-scale superconducting racetrack coil fabricated using epoxy impregnation technology and copper stabilized NbTi windings. This report focusses on the work carried out on racetrack and solenoidal NbTi magnets and components operating at liquid helium temperatures. (A separate report has been prepared on the High Tc work carried out under the amendment.)

During this contract on the development of the NbTi based magnet technology, the following results were achieved:

- An epoxy impregnated racetrack coil with mean length 52 cm, mean width 15 cm and section 4 cm x 4 cm was successfully fabricated inside a sealed, welded stainless steel frame (SS304L). The design strength was 400,000 Amp-turns.

- With the coil and frame immersed in liquid helium, the racetrack magnet trained to within a few percent of the short sample critical current and could be repeatedly quenched without damage. The peak average current density was estimated to be ≈ 350 A/cm^2 at a peak magnetic field in the windings of ≈ 6.8 Tesla. The magnet strength at the peak operating current (789 A) was 510,000 A-turns.

• Strain gauges suitable for liquid helium operation were selected and tested, and techniques for measuring strain in the temperature range 4.2 K to 300 K were developed. A modified Karma alloy type was used, and by employing pairs of gauges in dummy and active configuration, it was possible to measure actual strain after correction for apparent strain induced by thermal contraction and magneto-resistance effects. As a calibration test of these methods, the Young's Modulus of a stainless steel sample (SS 304L) was measured at cryogenic temperatures and found to agree with the tabulated values to within 2%.

• Measurements were made of the strain induced in a solenoidal superconducting magnet frame while the coil inside the frame was being energized at 4.2 K. Although the induced strain was observed to increase with the applied current, there were erratic jumps which made the data difficult to interpret. These jumps were due possibly to Lorentz force induced separation between the impregnated windings and the external SS304L magnet frame, where the gauges were installed.

• Measurements were made of the strain induced normal to the straight sides of the integrated racetrack coil and frame, as this coil was being energized at 4.2 K. A reversible, quadratic relationship between this strain and the coil current was observed. This is expected since the Lorentz force is proportional to the square of the current. Strains of 0.4% were recorded for the peak current application, which is considerably above that recommended for epoxy impregnated windings (the literature recommends that the peak strains in the winding should be maintained < 0.25%). (Note that with this racetrack coil and frame , the straight sides of the frame were <u>not</u> tied together as is commonly done with this type of construction to limit lateral strain.)

• Two types of thermally operated, superconducting persistent switches were modelled, designed and fabricated, and both the solenoidal and racetrack coils were tested while in persistent mode using these switches. The switches were driven normal by built-in resistive heaters. The first type of switch utilized the same 2:1 Cu:NbTi wire as the superconducting coils, and had a relatively low resistance while in the normal state at 15K ($\approx 10^{-2}$ ohm). This switch was tested with the racetrack coil, and stable persistent mode behaviour was obtained with an operating current of ≈ 650 A. A drop in persistent current of 3.9 % in 8 hours was observed, leading to an estimated total circuit (joint) resistance of 2.1×10^{-7} ohm.

• The second switch was fabricated using multiple strands of commercial switch wire stabilized by Cupro-Nickel 30 alloy in the ratio CuNi:NbTi=1.5:1. This had a much higher normal state resistance of 1.2 ohm at 15 K. This switch could operate stably for currents up to 475 A, but displayed instability above this value (e.g. the persistent mode would be stable at ≈ 650 A for 5-10 minutes and then the switch would quench). The lack of stability with this switch at the higher currents may have been due to several reasons: (a) the generally lower stability of the CuNi-stabilized switch wire when compared with the copper stabilized wire (b) lower quality fabrication of the switch (e.g. more voids etc). In the magnet design study contract , a CuNi: NbTi ratio of 3:1 was recommended. Unfortunately, there was

insufficient time left in the present contract to optimize the performance of the high resistance switch fabrication technology.

From the results summarized above, it was concluded that:

(a) The epoxy impregnation technology developed prior to the present contract could be successfully applied to fabricate high quality, lightweight, superconducting magnets of racetrack form;

(b) Racetrack magnets mounted in SS304L support frames could be fabricated which could successfully tolerate Lorentz force-induced lateral strains of up to 0.4%;

(c) Low resistance persistent switches could be fabricated to provide stable performance at coil operating currents up to at least 700 A.

(d) High resistance switches (R_{normal} > 1 ohm) could be fabricated to operate stably for coil currents up to 475 A. For higher currents, further investigations are required, e.g. using the same switch wire but with a larger safety factor per strand.

Sommaire

Le présent rapport fait état d'un contrat de recherche et de développement intitulé: "Fabrication et essai d'une bobine supraconductrice - Phase 3 du programme de développement Maglev". Les travaux ont été subventionnés par le Centre de développement des transports du Canada (CDT) et réalisés par la société CTF Systems, Inc., Port Coquitlam, Colombie Britannique.

Les travaux de recherche se rapportent au programme Maglev canadien, projet de R&D à long terme visant la mise au point d'une technologie de transport par sustentation dans des corridors de circulation choisis du Canada. Il faudra certainement attendre plusieurs décennies avant qu'un tel système soit économiquement réalisable dans le contexte canadien. C'est pourquoi il a été décidé d'adopter une stratégie qui consistera à maintenir un niveau relativement modeste de R&D en sustentation magnétique, juste assez pour former et maintenir des compétences canadiennes aptes à exploiter le Maglev lorsque la nécessité s'en fera sentir et en vue de réaliser des bénéfices économiques à court terme dans le domaine des transports et autres technologies naissantes.

Dans ce contrat, l'accent a été mis sur la mise au point industrielle d'une technologie de fabrication d'aimants supraconducteurs, de bobines supraconductrices et d'interrupteurs persistants pouvant fonctionner à une température de 4,2 K. Il s'agit de la poursuite des travaux réalisés sur les bobines cylindriques et dont les résultats apparaissent dans le rapport de Transports Canada intitulé: "Fabrication and Testing of Reduced-scale Superconducting Magnet" TP 7949E, et préparé par CTF Systems en juillet 1986.

Le projet avait pour objectif de fabriquer, d'essayer et d'évaluer une bobine supraconductrice de forme ovale entièrement instrumentée et réalisée selon les techniques d'imprégnation de résine époxydique élaborées lors de travaux antérieurs. Pendant l'exécution du contrat, la découverte extraordinaire des supraconducteurs à température critique élevée (Tc élevée) nous a incité à modifier les termes du contrat de manière à y inclure certains travaux sur les matériaux à température élevée. Les modifications au contrat ont été approuvées après la mise au point concluante d'un prototype à demi-échelle d'une bobine ovalisée supraconductrice en NbTi stabilisée au cuivre et imprégnée de résine époxydique et équipée des appareils de mesure requis. Ce rapport met l'accent sur les aimants et composants de type NbTi ovalisés et cylindriques fonctionnant aux températures de l'hélium liquide.

Dans le cadre du contrat sur la mise au point d'une technique de fabrication d'aimants de type NbTi, les résultats suivants ont été obtenus:

- Fabrication concluante d'une bobine ovalisée, imprégnée de résine époxydique, d'une longueur moyenne de 52 cm, d'une largeur moyenne de 15 cm et de section carrée de 4 cm x 4 cm. La bobine a été mise en forme dans un cadre en acier inoxydable soudé et scellé (SS 304L). Sa force nominale était de 400 000 A/tr.

- La bobine et le cadre ayant été plongés dans l'hélium liquide, l'aimant ovalisé a été amené par traînage à quelques pour-cent près du courant critique mesuré sur de petits échantillons et a subi plusieurs transitions sans dommage. La plus forte densité moyenne de courant de crête a été évaluée à $\approx$ 350 A/cm^2 dans un champ magnétique de pointe en bobinage de 6,8 tesla. La force de l'aimant au courant maximal de fonctionnement (789 A) était de 510 000 A/tr.

- Des extensomètres adaptés au fonctionnement dans l'hélium liquide ont été choisis et mis à l'essai. De même des techniques de mesure de déformation à des températures variant entre 4,2 K et 300 K ont été mises au point. C'est à partir d'un type d'alliage Karma modifié et en utilisant des paires de compteurs en configurations fictive et active, qu'il a été possible de mesurer les déformations réelles après correction de la déformation apparente induite par les effets de la contraction thermique et de la magnétorésistance. Pour vérifier ces méthodes, le moule SS 304L de Young a été mesuré à des températures cryogènes et les résultats obtenus se sont révélés conformes aux valeurs calculées à 2 p.100 près.

- On a effectué des mesures de la déformation induite dans le cadre de l'aimant supraconducteur de forme cylindrique au moment où la bobine était excitée à 4,2 K. Même si les chercheurs ont observé que la déformation induite augmentait en fonction du courant appliqué, il s'est produit des sauts irréguliers qui ont compliqué l'interprétation des données. Ces sauts étaient probablement causés par les séparations induites par effets Lorentz entre les enroulements imprégnés et le cadre extérieur SS 304L de l'aimant où les extensomètres étaient installés.

- Les experts ont mesuré la déformation induite normale aux côtés droits de l'ensemble bobine-cadre ovalisé pendant que la bobine était excitée à 4,2 K. Ils ont observé une relation quadratique et réversible entre cette déformation et le courant dans la bobine. Cette observation était prévisible puisque l'effet Lorentz est proportionnel au carré du courant. Des déformations de 0,4 p.100 ont été relevées au courant de pointe, valeur considérablement supérieure à celle qui est recommandée pour les enroulements imprégnés de résine époxydique. (Les ouvrages de référence dans ce domaine recommandent de maintenir à 0,25 p.100 les déformations maximums dans les enroulements. On notera, dans le cas de la bobine ovalisée et de son cadre, que les côtés droits du cadre n'étaient pas reliés comme c'est généralement le cas dans ce type de configuration pour limiter les déformations latérales.)

- On a modélisé, conçu et fabriqué deux types d'interrupteurs supraconducteurs persistants à commande thermique; les bobines de forme cylindrique et ovalisée ont été mises à l'essai en mode persistant avec ces deux interrupteurs. Les interrupteurs ont été activés normalement à l'aide de résistances chauffantes intégrées. Le premier type d'interrupteur était fabriqué avec le même file 2:1 Cu:NbTi que les bobines supraconductrices et offrait une résistance relativement faible en fonctionnement normal à 15 K ($\approx 10^{-2}$ ohm). Les experts ont fait l'essai de cet interrupteur avec la bobine ovalisée et ils ont obtenu un comportement stable en mode persistant avec un courant nominal de $\approx$ 650 A. Une baisse de courant persistant d'à peine 3.9 p.100 a été observée en huit heures de fonctionnement. Cela a permis d'évaluer la résistance totale du circuit à $2{,}1 \times 10^{-7}$ ohm.

- Le deuxième interrupteur était constitué de torons multiples de fil commercial d'interrupteur stabilisé par un alliage de cupro-nickel 30 dans une rapport de CuNi:NbTi=1.5:1. Cet alliage présentait une résistance beaucoup plus élevée à l'état normal, soit 1,2 ohm à 15 K. Cet interrupteur pouvait fonctionner de façon stable jusqu'à 475 A. Il était instable au-delà de cette valeur (par exemple, le mode persistant pouvait être stable à$\approx$650A pendant 5 à 10 minutes, après quoi l'interrupteur subissait une transition). Le manque de stabilité de cet interrupteur à des courants élevés peut avoir plusieurs causes: a) stabilité généralement plus basse du fil stabilisé au CuNi de l'interrupteur comparativement au fil stabilisé au cuivre; b) qualité de fabrication inférieure de l'interrupteur (un plus grand nombre de vides, etc.). Dans le contrat d'étude de conception de l'aimant (rapport du CDT sur la phase 1 du projet Maglev, TP 5436E), un ratio CuNi:NbTi de 3:1 avait été recommandé. Malheureusement, l'échéancier du présent contrat n'a pas permis d'optimiser la technologie de fabrication de l'interrupteur à résistance élevée.

Compte tenu des résultats résumés ci-dessus, voici nos conclusions:

a) la technique d'imprégnation à la résine époxydique élaborée avant l'exécution du présent contrat pourrait être appliquée avec succès dans la fabrication d'aimants supraconducteurs ovalisés légers et du haute qualité;

b) les aimants ovalisés montés dans des cadres SS 304L pourraient être fabriqués de manière à pouvoir supporter des déformations latérales induites par effet Lorentz jusqu'à 0,4 p.100;

c) des interrupteurs persistants à faible résistance pourraient être fabriqués pour assurer une performance stable aux courants nominaux de fonctionnement jusqu'à au moins 700 A;

d) des interrupteurs à résistance élevée ($R_{normale} > 1$ ohm) pourraient être fabriqués pour fonctionner de façon stable à des courants d'induction pouvant atteindre 475 A. Il faudrait poursuivre les recherches sur le fonctionnement de ces interrupteurs à des courants plus élevés, c'est-a-dire en utilisant le même type de fil, mais avec un plus grand facteur de sécurité par toron.

TABLE OF CONTENTS

Page

1. Introduction 1
   - 1.1. Background 1
   - 1.2. Scope of the Contract 1
   - 1.3. Contract Amendment 2

2. Characterization of Strain Gauges at Cryogenic Temperatures 4
   - 2.1. Test Apparatus 4
   - 2.2. Cryogenic Tests on Stainless Steel Samples (Type SS304L) 6

3. Strain Gauge Tests on a Superconducting Solenoid 9
   - 3.1. Instrumentation of Solenoidal Coil Frame 9
   - 3.2. Results of Cooldown to 4.2 K 9

4. Magnetic Field Computations 13
   - 4.1. Solenoidal Coil 13
   - 4.2. Racetrack Coil 14

5. Racetrack Coil Design, Fabrication and Testing 19
   - 5.1. Coil Design 19
   - 5.2. Coil Frame Design 20
   - 5.3. Coil Winding and Impregnation 22
   - 5.4. Strain Gauge Instrumentation 23
   - 5.5. Results of Liquid Helium Testing 25
     - 5.5.1. Training Performance 25
     - 5.5.2. Measurement and Interpretation of Transverse Strain 27

6. Persistent Switch 31
   - 6.1. Persistent Switch Design 31
   - 6.2. Fabrication of Persistent Switches 39
   - 6.3. Tests of PCS# 1 at Liquid Helium Temperatures 41
   - 6.4. Operation of Superconducting Coils in Persistent Mode 42

7. Conclusions 46

References 48

Page

List of Tables

Table 2.1 : Typical Strain Gauge Properties 6
Table 2.2 : Strain Gauge Information 6
Table 5.1: Coil and Wire Parameters for Racetrack Magnet 20
Table 5.2: Impregnation conditions for the racetrack coil winding 22
Table 6.1: Persistent Current Switch Simulation Parameters 35
Table 6.2: Persistent Current Switch Parameters 40
Table 6.3: Summary of Persistent Mode Tests 45

List of Figures

Fig. 2.1: Properties of strain gauges suitable for cryogenic measurements 5
Fig. 2.2: (a) Sketch of the strain estimation apparatus inserted in a dewar 7
(b) View of sample connected to the load via the steel cable with dummy gauge alongside. 7
Fig. 2.3: Electrical network for strain measurement 7
Fig. 2.4: Apparent strain of Karma alloy gauge during cooldown to 4.2K (measured using a Wheatstone bridge network). 8
Fig. 2.5: Stress strain data for a stainless steel sample (SS 304L) 8

Fig. 3.1 Superconducting solenoidal magnet dimensions. 9
Fig. 3.2 : Location of strain gauges on the solenoidal coil frame. 10
Fig. 3.3: Normalized strain vs coil current for active and dummy gauge pair A1 and D1. 11
Fig. 3.4: Normalized corrected strain (A3-D3) vs coil current for gauge pair A3 and D3. 11

Fig. 4.1: Geometry of solenoidal coil current carrying element dl and field point P. 13
Fig. 4.2 : Comparison of the axial magnetic fields (Bz in Tesla) vs median radius (cm) computed using Hart's Tables [5] and the software written using Hart's magnetic field formulation, for a solenoid with the listed parameters 14
Fig. 4.3 : Contours of axial field Bz in the x-z plane for a solenoid of inner radius 12.93 cm, outer radius 16.92 cm, and length 3.89 cm 15
Fig. 4.4 : Pictorial representation in 3-dimensions of the field contours of Bz (vertical axis) in the x-z plane for the solenoid parameters listed in Fig. 4.3 caption 15
Fig. 4.5: Racetrack coil and coordinate system. 16
Fig. 4.6: Bz (gauss/ampere) vs x (cm) for a racetrack coil with the indicated parameters 16

		Page
Fig.4.7:	Bz (gauss/ampere) vs y (cm) for a racetrack coil with the indicated parameters	17
Fig.4.8:	Bz (gauss/ampere) vs z (cm) for a racetrack coil with the indicated parameters	17
Fig. 4.9 :	Contours of Bz (vertical axis) on the median x-y plane of a racetrack coil with the dimensions indicated in Figs 4.7-4.9.	18
Fig. 5.1 :	NbTi Jc vs field data [6], reduced by 2:1 Cu: NbTi ratio and coil fill factor of 80%, in relation to the coil load line for the peak field at the inner coil radius on the coil x axis (Fig. 4.5).	21
Fig. 5.2:	Racetrack coil winding and support frame from SS304L.	21
Fig. 5.3:	Winding pattern used for the racetrack coil	22
Fig. 5.4:	View of completed racetrack coil, SS304L frame and current lead bus bars	23
Fig. 5.4:	(a) Top view of strain gauge location for the racetrack coil measurements.	24
	(b) Side sectional view of locations of gauge pairs A1/D1, and A2/D2	24
Fig. 5.5 :	Racetrack coil mounted in liquid helium test dewar.	25
Fig. 5.6 :	(a) Training critical current vs trial number.	26
	(b) Critical current density vs trial number	26
Fig. 5.7	(a) Strain (μm/m) vs coil current for the gauge pair on the top brass strip (A1/D1).	28
	(b) Strain (μm/m) vs coil current for the gauge pair on the bottom brass strip (A2/D2)	28
Fig. 5.8	Lateral load density vs x for the racetrack parameters indicated	29
Fig. 5.9	Model of coil and frame for the strain estimation	30
Fig. 6.1	Circuit for Superconducting coil and persistent switch	31
Fig. 6.2:	Persistent switch model	34
Fig. 6.3	(a) Supply and superconducting coil voltage vs time.	36
	(b) Superconducting coil voltage vs time.	36
	(c) Current through PCS and protection resistor vs time.	37
	(d) Power dissipation in switch and heater and cooling power of LHe bath on switch vs time.	37
	(e) Liquid helium loss during operation of switch vs time	38
	(f) Resistivity of sc wire copper stabiliser vs time	38
	(g) Switch temperature vs time	39
Fig. 6.4:	Comparison of theory and experiment for PCS#1 and racetrack coil.	41
Fig. 6.5	Arrangement of superconducting coil and PCS.	42
Fig. 6.6:	View of physical arrangement of racetrack coil and frame and PCS#1	43
Fig. 6.7:	View of physical arrangement of solenoidal coil and frame and PCS#2	43
Fig. 6.8:	Experimental record of Hall probe magnetometer (coil supply current) and Vcoil(t) for the racetrack magnet and PCS#1 for starting current = 645 A.	44

1. INTRODUCTION

1.1. Background

The Transportation Development Centre of Transport Canada (TDC) has sponsored a series of R &D investigations into high speed transportation systems involving a superconducting Maglev technology with non-contact magnetic suspension and propulsion. During the past 18 years of Maglev activity in Canada, there have been a number of studies and developments of both the technical and economic issues associated with the implementation of such a system in the Toronto-Ottawa-Montreal corridor [1][1]. Although it is unlikely that such a system will be required in Canada before the early decades of the 21st century, TDC has deemed it appropriate to maintain a modest level of R&D activity in this area both to provide expert technical advice to the government on Maglev, and also in the anticipation of some nearer term spin-off benefits to transportation and other emerging technologies.

CTF Systems Inc. has been involved in various cryogenic aspects of superconducting Maglev technology including analyses of Maglev cooling systems [2], superconducting magnet design [3], and superconducting magnet development [4]. In the previous R&D phase [4], CTF Systems developed a fabrication technology for lightweight, epoxy-impregnated superconducting magnets. The process was tested with a solenoidal (circular) coil mounted in a SS304 L frame. In the present contract activity described in this report, the work has been extended to racetrack-shaped coils and also to the development and testing of high current persistent switches for operation of the superconducting magnets in persistent mode, i.e. without an external power supply to maintain the coil current.

1.2. Scope of the Contract

The model objective as specified in the initial contract work statement was as follows:

> "To ensure that full advantage is taken of advanced non-contact vehicle suspension and propulsion technology to maintain a modern, efficient and socially acceptable Canadian transportation system".

The sub-objective relating to the Candian EDS Maglev System was:

> " To operationally deploy an electrodynamic magnetically levitated and linear synchronous motor propelled high speed guided ground transportation system in the Canadian corridor".

[1] Numbers in square brackets [ ] are references listed at the end of the report

The elements of the initial detailed statement of work can be outlined as follows:

1.2.1 Develop a detailed plan of work, activity schedule, cash flow projection, project management control, and documentation procedures within three (3) weeks of effective commencement date
1.2.2 Collate all pertinent data from previous work and knowledge gathered
1.2.3 Purchase superconducting wire and impregnation materials
1.2.4 Modify racetrack coil drawings to current configuration
1.2.5 Adapt racetrack coil frame drawings to current configuration
1.2.6 Establish sub-contractor agreements
1.2.7 Design and fabricate appropriate jigging and fixtures
1.2.8 Fabricate racetrack coil frame
1.2.9 Test insert design and drawings
1.2.10 Evaluate and refine persistent switch
1.2.11 Evaluate strain transducer
1.2.12 Test insert fabrication and assembly
1.2.13 Fabricate face plate seal
1.2.14 Wind coil
1.2.15 Impregnate superconducting coil
1.2.16 Test dewar and insert
1.2.17 Test racetrack coil in dewar
1.2.18 Make modifications deemed necessary and repeat testing
1.2.19 Analyse and document results
1.2.20 Prepare and deliver to TDC 30 copies of a technical report describing the work carried out and the results achieved.

1.3. Contract Amendment

During 1986 and early 1987, high temperature (high Tc) superconductors were discovered with critical temperatures up to 93 K [5]. This fascinating discovery prompted much speculation about the impact of the high Tc superconductors on many applications of superconductors including superconducting Maglev. After some consultations with TDC, an amendment to the initial contract was granted, involving investigation of several aspects of high Tc superconductors with particular relevance to transportation technology. It was decided to:

(1.1) Complete the work on the design, fabrication and testing of a reduced scale racetrack coil fabricated with conventional "low Tc " superconductors;
(1.2) Complete the development and testing of persistent current switches for operation (in persistent mode) of the developed superconducting coils;
(1.3) Prepare a report describing this activity.

Once the activity with the racetrack magnet and persistent switches had been brought to a satisfactory level, then the balance of activity was to be channeled to the high Tc area, in particular with the general goals of :

(2.1) Gathering and assessing information on high Tc developments;
(2.2) Fabricating and testing short samples of high Tc wire;
(2.3) Investigating of the impact of high Tc materials on Maglev and any other technologies relevant to transportation interests.

The work summarized in 1.1 and 1.2 above is outlined in detail in this report. A separate report has been prepared on the work elements 2.1-2.3 carried out during the high Tc amendment.

2. CHARACTERIZATION OF STRAIN GAUGES AT CRYOGENIC TEMPERATURES

The contract work statement required the characterization of strain gauges for monitoring the strain induced in the magnet coils and coil frames during energising. Gauges for magnet strain characterization have been selected and tested over the temperature range 300K- 4.2 K. This chapter describes the characterization tests performed on the selected gauges.

2.1. Test Apparatus

The most widely used strain estimation method involves the measurement of the change of resistance with applied strain. Two problems which have to be addressed in the use of resistive strain gauges in a cryogenic environment are:

(a) All gauge materials contract during cooldown and the gauge will thus display apparent strain signals related to the cooldown temperature range. The apparent strain signal depends on the gauge and backing materials.
(b) Most gauge materials display a magnetic field dependent resistivity. This results in an apparent signal which has to be distinguished from the true strain during coil energizing.

A useful review of the general behaviour of strain gauges for cryogenic measurements has been given by L.L. Sparks [6]. Two major types of gauges have been considered: (a) Platinum-tungsten(Pt-W) and (b) Modified Karma Alloy. Some of their reported properties are indicated in Figs 2.1(a) and 2.1(b) In Figure 2.1(a) the apparent strain vs temperature curves for six gauges of modified Karma alloy (nickel-chromium), are indicated for temperatures between 300K and 4.2 K. The magnetic field dependence is indicated in Figure 2.1(b) at 4.2Kfor both the Pt-W and Karma alloy gauges for fields in the range $0 < B < 8$ T.

From the literature, several points are clear:

- In the vicinity of 4.2 K, the Pt-W gauges have a much smaller apparent strain dependence with temperature (10ppm/K) than the Karma type (150 ppm/K). This indicates that temperature stability during measurement is an important concern with the Karma alloy type.
- In the vicinity of 4.2 K, the Pt-W gauges are much less sensitive to magnetic fields up to 8 Teslas. The Karma gauges have a reproducible magneto-resistance which is linear in high field ($3 < B < 12$ T),roughly quadratic in low field ($0.5<B<3$ T) and is independent of field direction.
- On cooldown from 300 to 4.2K, modified Karma alloy gauges display a change of resistance of 0.15% vs 8% for Pt-W. Thus the Pt-W gauges are not appropriate for cooldown strain estimation. Note that there would be large errors with cooldown strain estimation even with the Karma alloy type since the 300K-4.2K thermal contraction of stainless steels is $\Delta L/L = \varepsilon \approx 0.28\%$.
- The gauge factors G ($= \partial R/\varepsilon R$) for both types, increase by 5-6% over their room temperature values.

- The Karma alloy gauges display negligible hysteresis in a wide range of strains (200-9000μm/m) and the accuracy in this range is about 10μm/m.

These properties are summarized in Table 2.1.

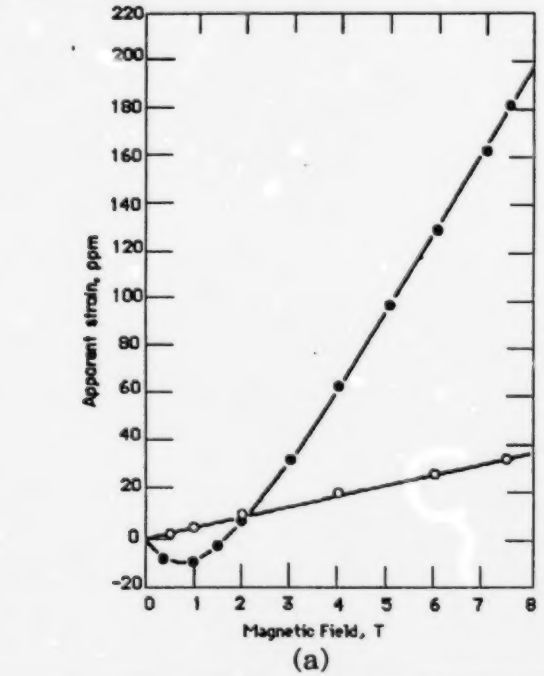

Fig. 2.1: **Properties of strain gauges suitable for cryogenic measurements. (a): Apparent syrain vs magnetic field at 4.22K ; open circles Pt-W, closed circles - modified Karma. (b) Apparent strain vs temperature for 6 modified Karma MM-WK-15-250BG-350 gauges [7].**

Table 2.1 : **Typical Strain Gauge Properties.**

Gauge Type	Pt-W	Mod. Karma
Gauge factor G	4.5	2.1-2.2
∂G/G (300-4.2K) (%)	+6	+5
Apparent Strain vs T at 4.2K		
dε/dT (ppm/K)	10	150
ΔR/R (300-4.2K) (%)	8	0.15

2.2. Cryogenic Tests on Stainless Steel Samples (Type SS304L)

In the interests of measuring cooldown- as well as Lorentz-induced strains, it was decided to employ the modified Karma alloy type gauges. Since the apparent cooldown strain for this gauge was known to vary within a given lot on the same substrate (Fig.2.1(a)), it was important to calibrate the gauges. The information on the gauges selected is listed in Table 2.2. An apparatus was constructed in order to gain some experience with the Karma alloy gauges, and to determine the accuracy with which one could estimate strain at room and cryogenic temperatures. This apparatus is indicated in Figure 2.2 (a) with a view in Fig.2.2 (b). It consisted of a spring scale connected via a steel cable to one end of a standard sample shape with the other end of the sample bolted to the opposite end of the apparatus. This sample end of the apparatus could be mounted in a suitable dewar for cooldown to liquid nitrogen and helium temperatures. A dummy sample was mounted alongside the strained sample in order to allow for compensation of the apparent thermal strain. Strain gauges from the same batch were mounted on each sample. Each gauge was connected in turn into one arm of a Wheatstone bridge (Fig. 2.3), and the difference in their readings at a given temperature taken as representing the true strain.

Figure 2.4. shows the apparent strain during cooldown for one such gauge, measured on two different occasions in very low magnetic field. The apparent strain and its rate of change are quite high in the vicinity of 4K, but for any one gauge are reasonably reproducible. Using this apparatus, the stress-strain curve for stainless steel SS304L at 4.2 K was measured (Fig. 2.5) and the Young's modulus E found to be in reasonable agreement with tabulated values: $E_{tabulated}(4.2K) = 29.2ksi$; $E_{measured}(4.2K) = 29.7 \pm 1.0ksi$.

Table 2.2 : **Strain Gauge Information**

Supplier :	Micro-Measurements Division, Measurements Group, P.O. Box 27777, Raleigh, N. Carolina, NC 27611, USA. (919) 365-3800
Gauge Models:	WK-13-250BG-350 : R(300K) = 350.0±0.3%; G(300K) = 2.18±1.0% WK-15-250BG-350 : R(300K) = 350.0±0.3%; G(300K) = 2.08±1.0%.
Bonding:	M-Bond 610 Adhesive Kit and 43-B Coating Kit

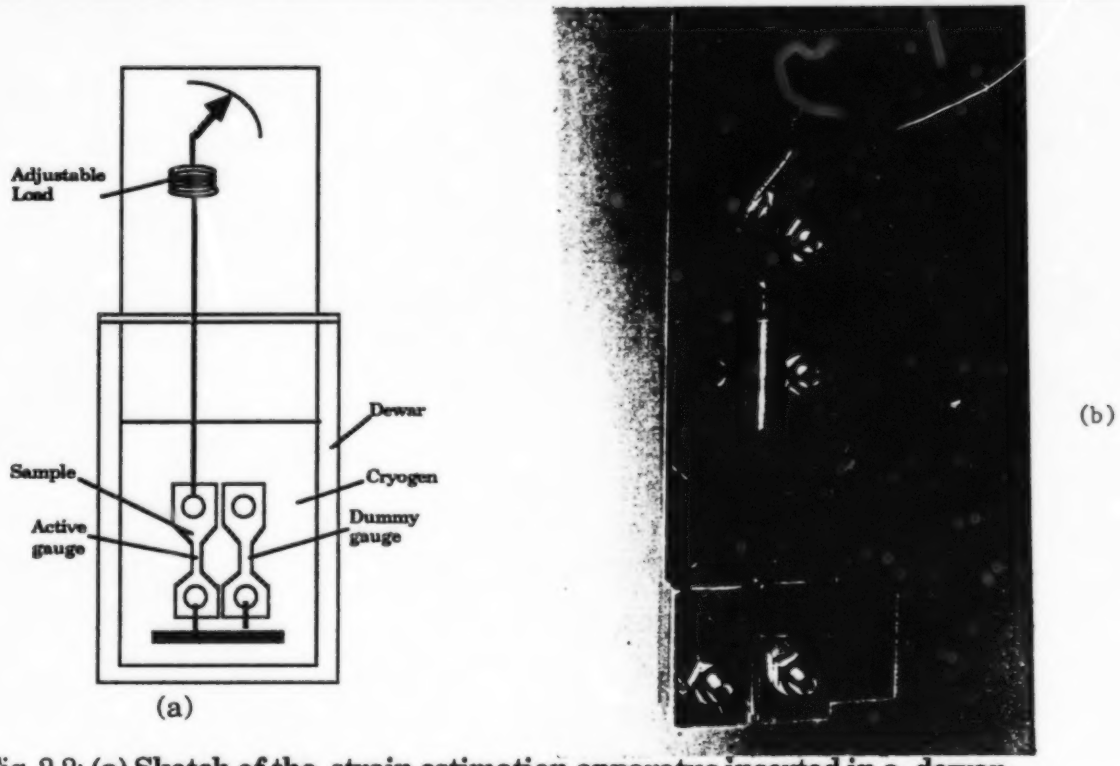

Fig. 2.2: **(a) Sketch of the strain estimation apparatus inserted in a dewar. (b) View of sample connected to the load via the steel cable with dummy gauge alongside.**

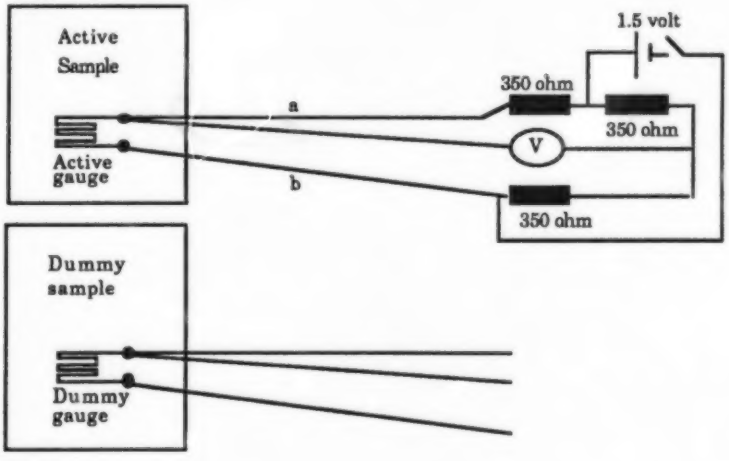

Fig. 2.3: **Electrical network for strain measurement.** Lines a and b have identical resistances. The 350 ohm resistances were adjusted to be 350 ± 0.1 ohm. The electrical circuit at 300 K was switched between the active and dummy gauges for the measurement.

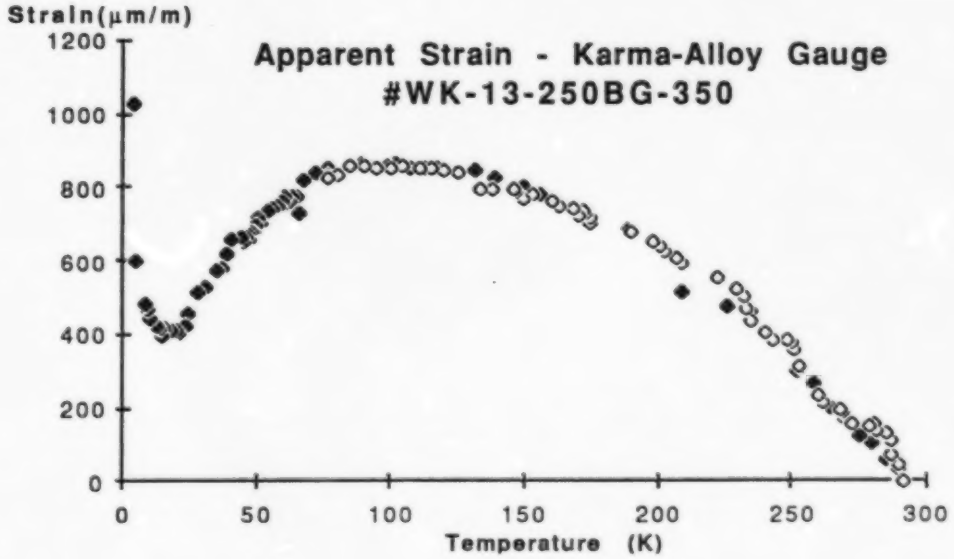

Fig. 2.4: **Apparent strain of Karma alloy gauge during cooldown to 4.2K (measured using a Wheatstone bridge network).** Data are shown for two different gauges from the same commercial fabrication batch.

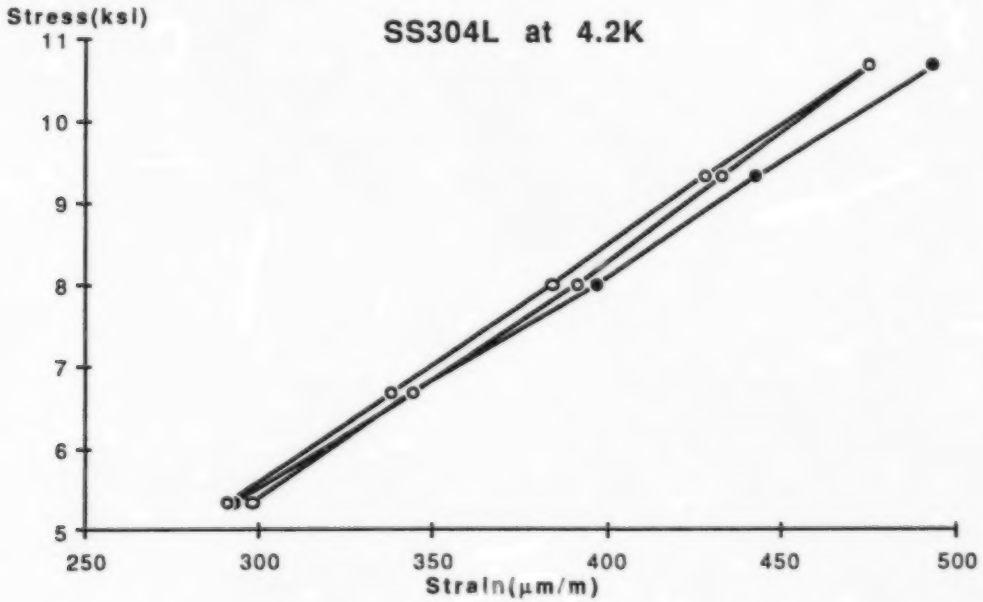

Fig. 2.5: **Stress strain data for a stainless steel sample (SS 304L).** The sample was pre-strained to a certain level in order to fully align the sample, gauge and tension direction. Spurious signals occurred if any bending took place during tensile loading. The data refer to two different cooldowns of the same sample.

3. STRAIN GAUGE TESTS ON A SUPERCONDUCTING SOLENOID

In order to establish the behaviour of the Karma alloy gauges on an actual superconducting magnet, a series of tests was carried out with active-dummy pairs of gauges applied to the superconducting solenoid which was developed and tested during a previous phase of the Canadian Maglev R&D activity [4].

3.1. Instrumentation of Solenoidal Coil Frame

The epoxy impregnated solenoidal coil had mean radius 15.0 cm, and section 4.0 cm x 4.0 cm, with design strength at 400,000 Ampere turns (KAT), for an operating current of 662 A. During testing, the coil had reached short sample critical current of 914 A for a peak strength of 552 KAT. The winding itself was mounted in a SS304L frame with cooling channels around the coil circumference. A section through the coil and frame in question is indicated in Fig. 3.1.

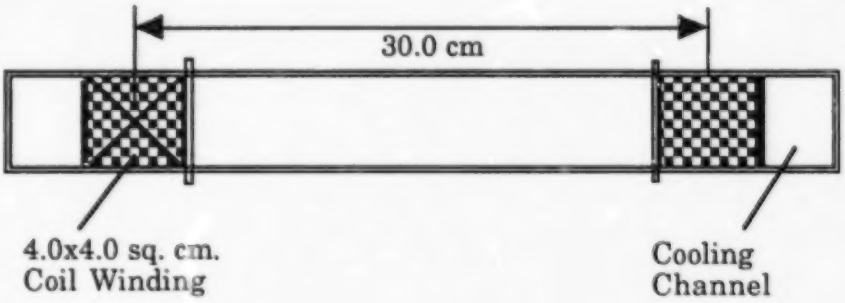

Fig. 3.1 **Superconducting solenoidal magnet dimensions.**

Three pairs of Karma alloy gauges (active and dummy) were mounted on the solenoidal coil frame, where they would be subjected to relatively large magnetic fields (> 1T) when the coil was operated at the design current. The active gauge was bonded directly to the SS304L frame while the dummy was mounted as close as possible on a separated strip of SS 304L, with its centre at the same radius as the active gauge. The active gauges were bonded to respond to radial forces. From symmetry considerations both gauges of a given active-dummy pair should have been subjected to almost the same magnetic field (Fig. 3.2). Thermometers were thermally anchored to the stainless steel surface to monitor the local temperature.

3.2. Results of Cooldown to 4.2 K

The data recorded during cooldown were not reproducible and will not be reported here. At 4.22K, the signals from active-dummy gauge pairs were monitored as the coil currents were increased with the coil at various temperatures. A typical data set at 4.2 K for the strain gauge pair A1 and D1 are shown in Figs. 3.3 . The measurements were repeated several times and indicated that the results were not very reproducible and often showed hysteresis especially at

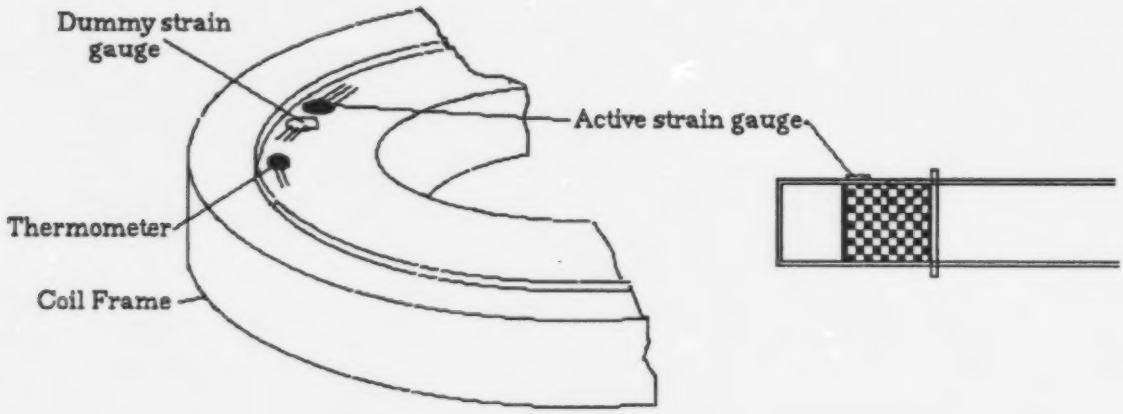

Fig. 3.2 : **Location of strain gauges on the solenoidal coil frame.** The active gauges were bonded to the stainless steel coil frame surface. The dummy gauges were bonded to a separate strip of SS304L, mounted as closely as possible to the active gauge, but were not affected by the coil frame strain.

the higher coil currents. Also included in the data of Fig. 3.3 are data reported in the literature for similar Karma alloy gauges (solid line). The total magnetic field at the gauge locations was computed using software developed for the purpose (chapter 4) and for the location of the gauges, represented a total field load load line of 0.005 Tesla/Ampere. This allowed the fit to the data reported by Walstrom [7].

One interpretation of the discontinuities in the 4.22K strain data is that the impregnated winding was moving (i.e.) slipping relative to the frame under the increasing Lorentz stress. This could have given rise to the sudden jumps in the strain at 200 and 400 A.

Fig. 3.4 is a plot of the actual strain estimated from the gauge pair A3 and D3, vs coil current. The strain is given by A3-D3 and these data also have discontinuities. Also plotted in Fig. 3.4 is an estimate of the strain induced in the coil composite by the Lorentz loading. This was determined by computing the displacement of the coil composite along the median radius as a function of coil current using the 2-dimensional stress formulation of Arp [8]. The coil had mean radius 75mm and square section of side 40mm. The effect of the coil frame was not included in the analysis. Although the analysis provides approximately the strain values measured, the variations preclude any statement about agreement between theory and experiment. Since the Lorentz force is proportional to the square of coil current I one expects a strain $\epsilon \propto I^2$.

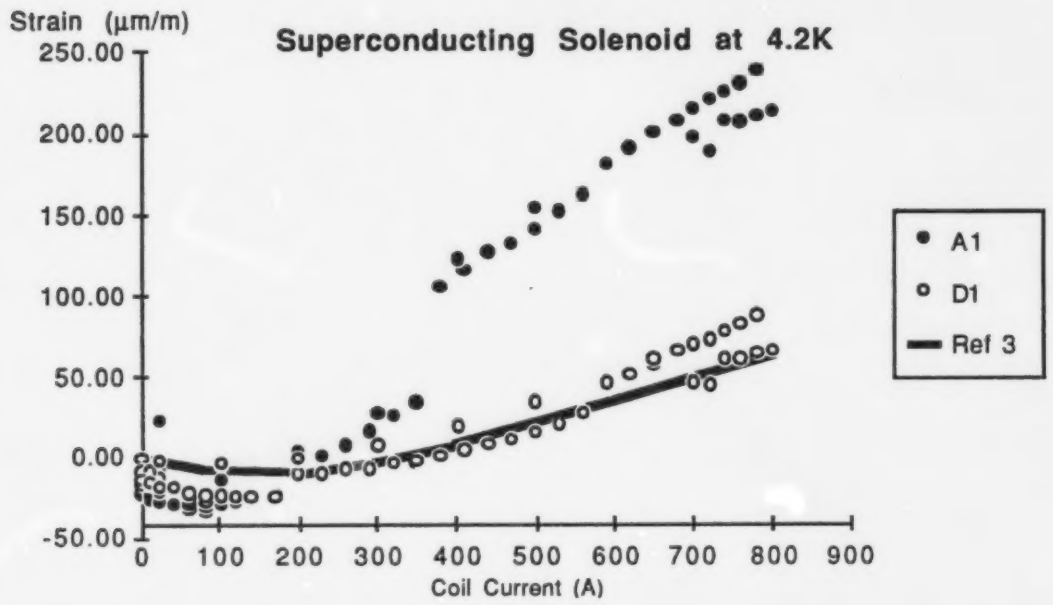

Fig. 3.3: **Normalized strain vs coil current for active and dummy gauge pair A1 and D1.** The solid line represents the data reported for Karma alloy gauges by Walstrom [7], fitted to the estimated total field applied to the gauges.

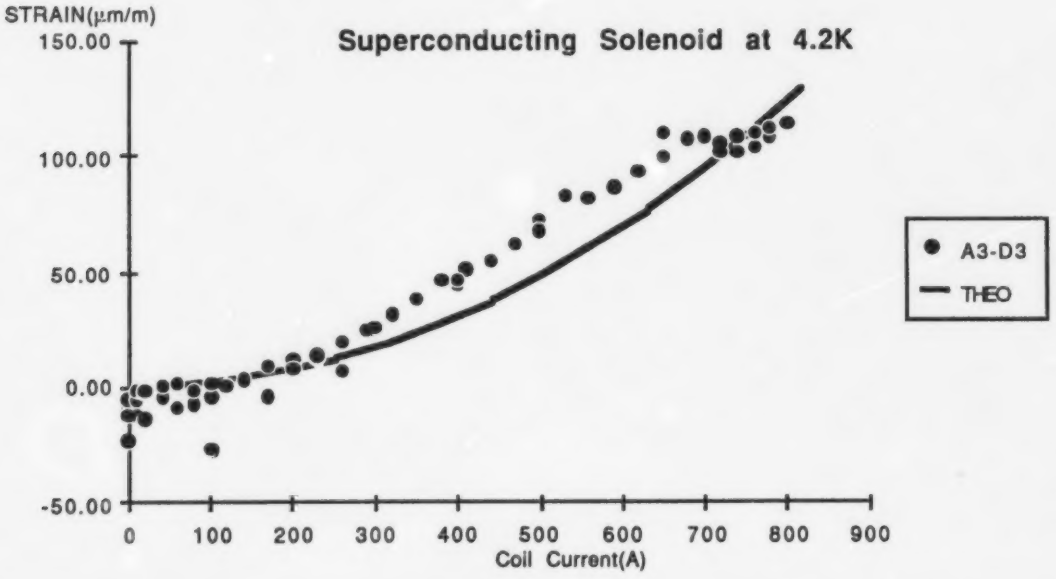

Fig. 3.4: **Normalized corrected strain (A3-D3) vs coil current for gauge pair A3 and D3.** The solid line represents an estimate of the expected strain at the coil maximum radius for the coil alone using the two-dimensional superconducting solenoid analysis of V. Arp [8].

It is clear from these experiments that the data are difficult to interpret, and this emphasizes the difficulty in measuring strain in a situation where coil slippage relative to the frame could occur. The experiments would have been more direct had the coil frame been removed and the gauges attached directly to the composite surfaces. However, with the present fabrication method, where the coil frame is designed to restrain the Lorentz loading, it was decided not to attempt to remove the frame, since it would have resulted in significant damage to the epoxy/wire composite and the magnet input leads. An alternative would have been to utilize the method employed for the racetrack magnet strain measurements (see section 5.5.2).

4. MAGNETIC FIELD COMPUTATIONS

During the course of the design of the frame for the racetrack coil, of the persistent switches, various experimental tests, and data analyses, it became important to acquire the ability to efficiently compute magnetic field components at any point in space relative to a specific coil. The magnetic fields of solenoidal and racetrack coils with distributed conductors were calculated using the Biot-Savart formula for the vector field contribution $\underline{dB}$ at a point P (x,y,z) due to a current I in some conductor vector element $\underline{dl}$ (Fig. 4.1):

$$\underline{dB} = \frac{\mu_0 \cdot I \cdot (\underline{dl} \times \underline{s})}{4\pi \cdot s^3} \qquad (4.1)$$

where $\underline{s}$ = distance vector from $\underline{dl}$ to the field point P, s is the scalar value of $\underline{s}$, and $\mu_0 = 4 \cdot \pi \cdot 10^{-7}$ webers/ampere·meter.

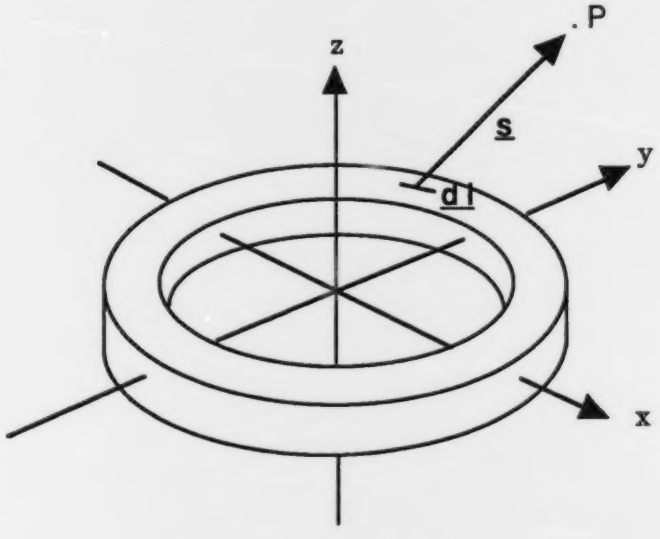

Fig. 4.1: **Geometry of solenoidal coil current carrying element $\underline{dl}$ and field point $\underline{P}$.**

4.1. Solenoidal Coil

Software was generated to compute the axial and radial field components of a solenoid with distributed current density distribution using the formulation outlined by Hart [9]. The Hart tables also provided a useful check on the accuracy of the generated fields for a given distribution. As an example of the calculations, Fig. 4.2 compares the fields listed in the Hart Tables with the software calculations for the superconducting solenoid fabricated during the previous Maglev project phase 2 [4]. The axial fields were computed for coordinates along the coil median radius from the coil centre, for a strength of 400 kilo-ampere turns. The agreement is better than 1/2% over the radius range selected.

The axial and radial fields were also computed for various coordinates relative to the coil. As an example, contours of Bz (in units of gauss/ampere) are indicated in Fig. 4.3 for a solenoid of the same parameters as Fig. 4.2 for coordinates in the median plane. A 3-dimensional representation of the data is indicated in Fig. 4.4. The generation of the contours was accomplished using contouring and graphics software available internally at CTF.

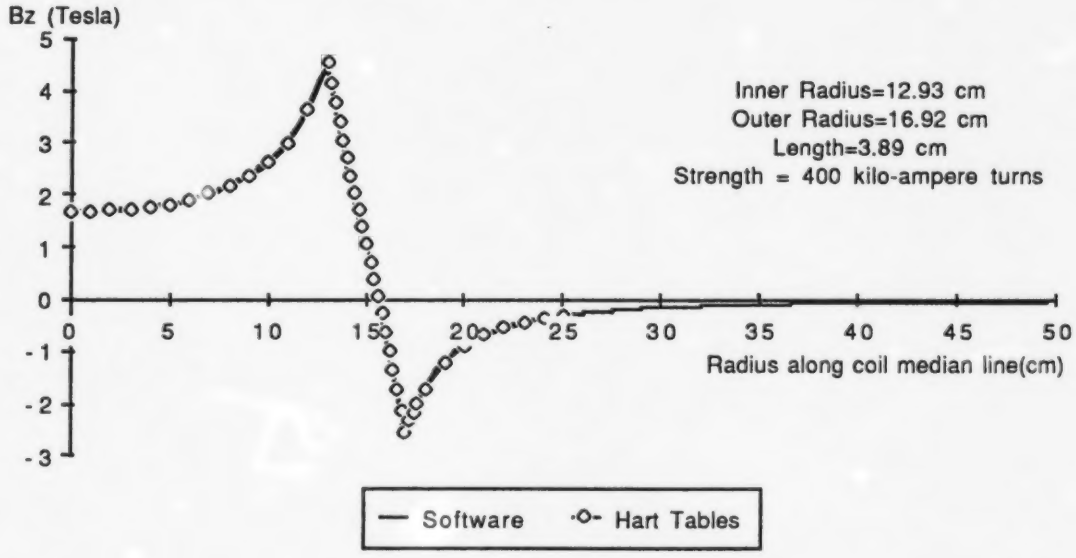

Fig. 4.2 : **Comparison of the axial magnetic fields (Bz in Tesla) vs median radius (cm) computed using Hart's Tables [9] and the software written using Hart's magnetic field formulation, for a solenoid with the listed parameters.**

4.2. Racetrack coil

Software was also generated for computation of the magnetic field at a general point P, due to a racetrack coil of geometry indicated in Fig. 4.5. The field components were generated by superposition of fields due to the two hemispherical ends and the two straight sides. Each of these 4 elements was subdivided into elements of length dl and section dy·dz. Calculations were carried out for the case of the racetrack coil which has been built during this phase (section 5). The magnitudes of the axial fields Bz in gauss/ampere along the x-, y-, and z-axes for distances to 50 cm from the origin at the coil centre are indicated in Figs 4.6, 4.7 and 4.8 rspectivey. As an example of 3-dimensional contour calculation, Fig. 4.9 presents contours of constant Bz in the x-y median plane.

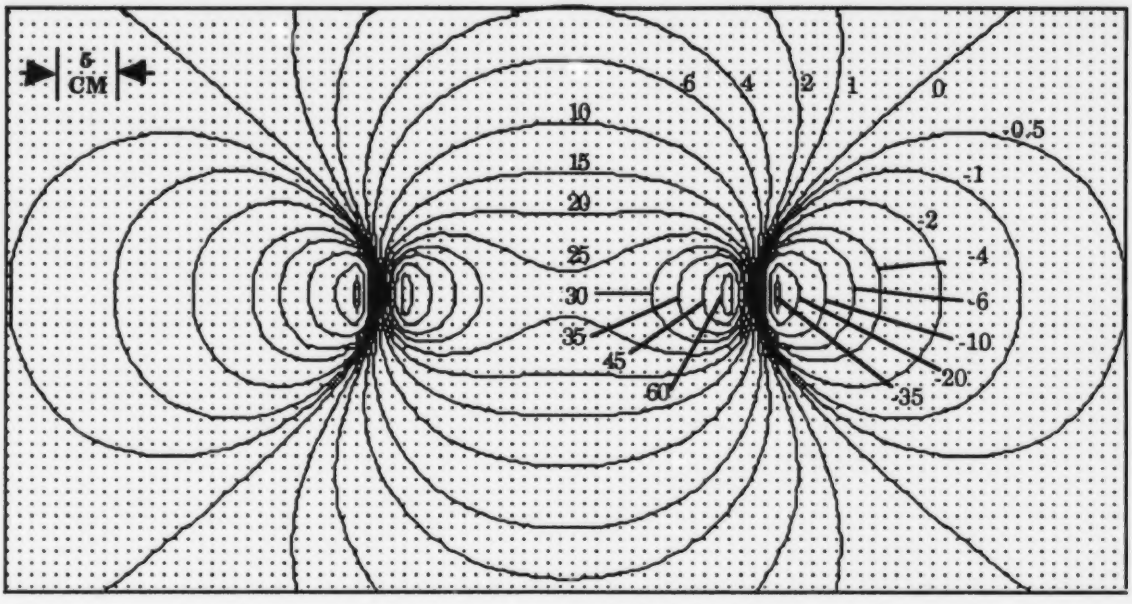

Fig. 4.3: **Contours of axial field Bz in the x-z plane for a solenoid of inner radius 12.93 cm, outer radius 16.92 cm, and length 3.89 cm.** The field contours are listed in gauss/amp and the dots are spaced by 1cm horizontally (x-axis) and vertically (z-axis).

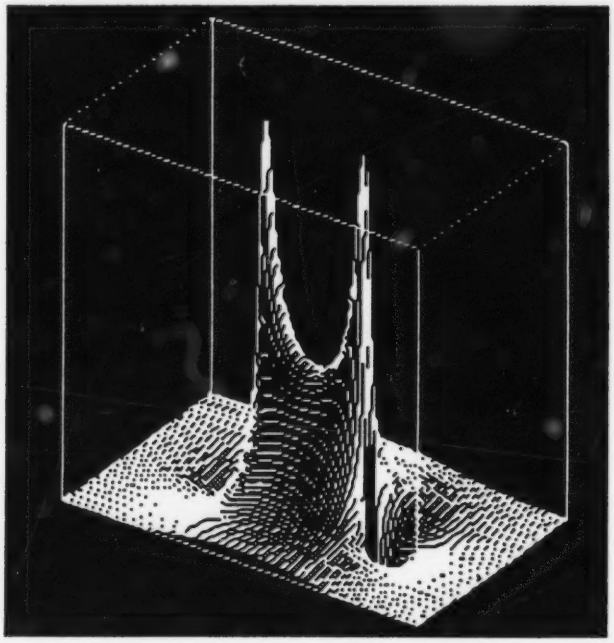

Fig. 4.4: **Pictorial representation in 3-dimensions of the field contours of Bz (vertical axis) in the x-z plane for the solenoid parameters listed in Fig. 4.3 caption.**

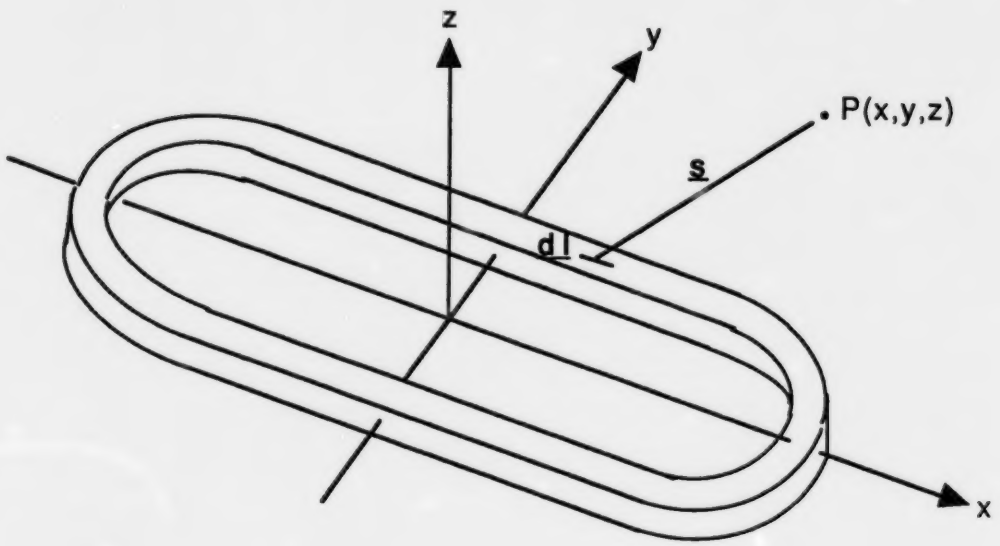

Fig. 4.5: **Racetrack coil and coordinate system.**

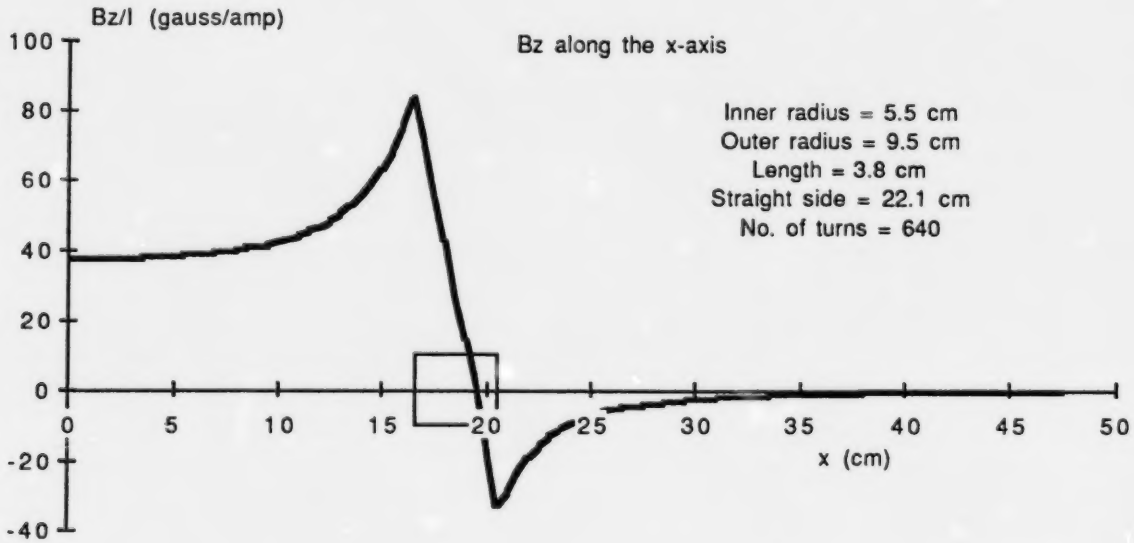

Fig. 4.6: **Bz (gauss/ampere) vs x (cm) for a racetrack coil with the indicated parameters.** The box indicates the conductor section location on the x-axis.

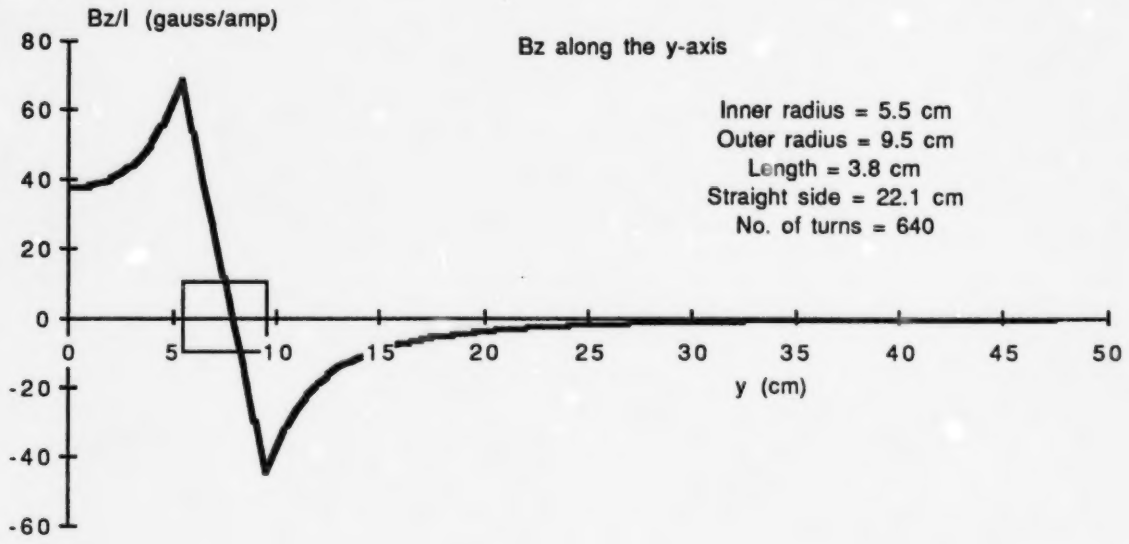

Fig.4.7: **Bz (gauss/ampere) vs y (cm) for a racetrack coil with the indicated parameters.** The box indicates the conductor section location on the y-axis.

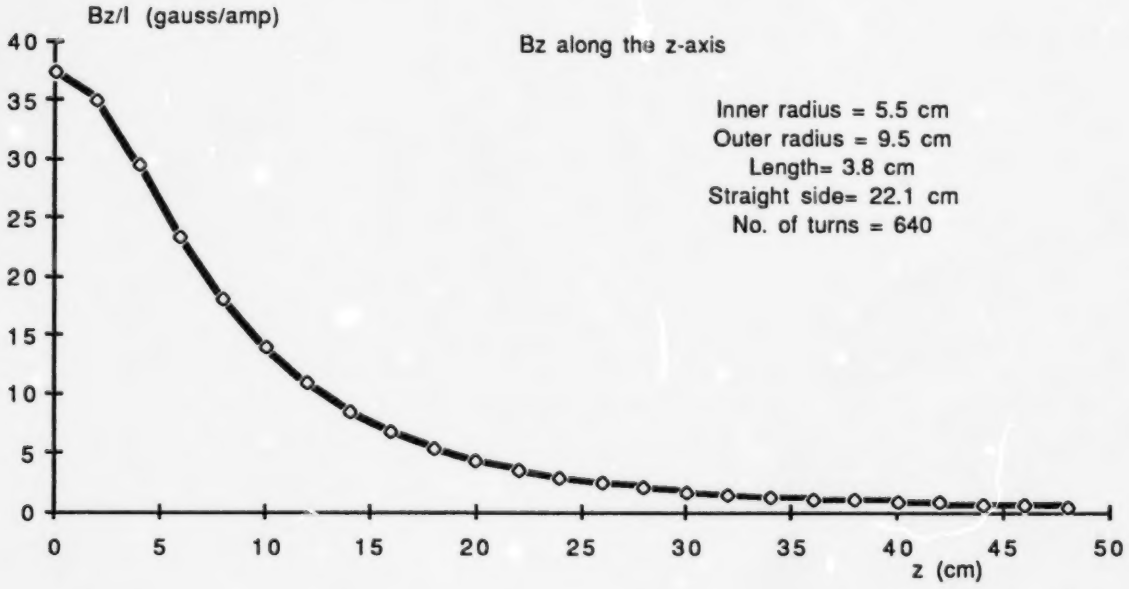

Fig.4.8: **Bz (gauss/ampere) vs z (cm) for a racetrack coil with the indicated parameters.**

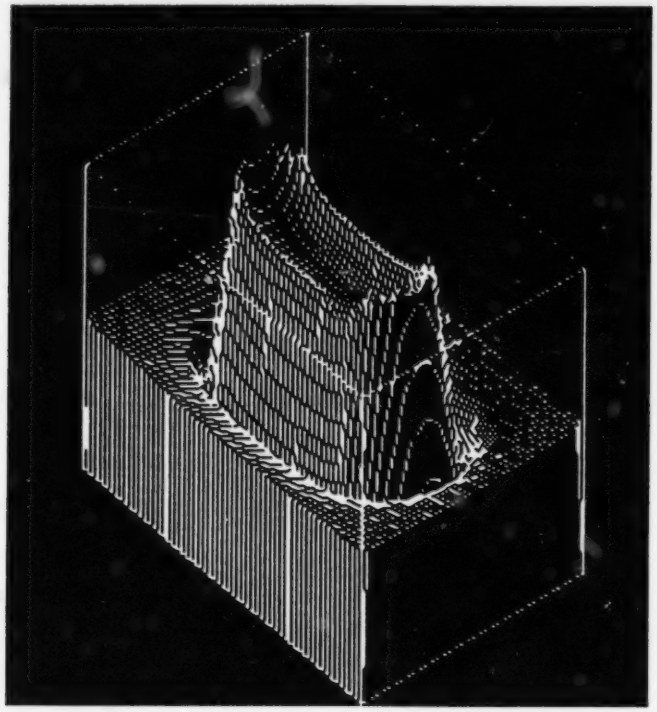

Fig. 4.9: **Contours of Bz (vertical axis) on the median x-y plane of a racetrack coil with the dimensions indicated in Figs 4.7-4.9.**

5. RACETRACK COIL DESIGN, FABRICATION AND TESTING

This chapter outlines the design, fabrication and testing of a racetrack coil mounted in a stainless steel frame (SS304L). The testing included a sequence of training runs and also strain measurements across the straight sides of the coil, as it was being energized at 4.2 K.

5.1. Coil Design

At the initiation of the contract, a survey of superconducting wire suppliers was undertaken, and it was discovered that the supplier of the wire for the previous Maglev contract phase 2 (Oxford Airco), could not deliver until 8-9 months after receipt of the order. Other vendors could supply wire sooner e.g. within 5-6 months, but with inferior characteristics, in particular a lower copper stabiliser residual resistivity ratio (RRR).

Various analyses were carried out concerning the projected performance of superconducting coils fabricated using wires from the alternative vendors, and it was concluded that it would be best to purchase the better quality Oxford Airco wire, since good training behaviour had been achieved in the performance of the solenoid constructed during the phase 2 contract [4]. In the interim, to gain experience in the fabrication and testing of racetrack coils, it was decided to fabricate a reduced scale coil using the superconducting wire from Oxford which remained after the Maglev Phase 2 contract.

The coil selected for fabrication was a half scale racetrack with the parameters indicated in Table 5.1. With the selected parameters, it was expected that the stresses within the winding would be more severe than with the larger levitation coil radius due to the stress during winding, and Lorentz stress during energizing. The smaller coil was thus expected to be a more severe test of the coil fabrication process. Peak magnetic fields at the coil inner end radius and at the inner median line on the straight side centre were computed from data similar to Figs. 4.6, and 4.7, which show the axial field variation along relevant directions outside and within the winding.

The load line of the racetrack coil for the peak field point in the winding (on the coil ends) is indicated in Fig. 5.1 relative to the critical current density (Jc) of NbTi reduced for a 2:1 copper:NbTi stabiliser ratio and an 80% coil fill factor. The data are plotted for three temperatures (4.2K, 4.5K, and 5.7 K). The Jc data for pure NbTi were taken from reference [10] , and were least squares fitted to provide a functional form of current density Jc vs field B (Tesla) and temperature T:

$$Jc(NbTi)[A/mm^2] = 4132 - 537 \cdot B + 15.6 \cdot B^2 - (845 - 54 \cdot B + 1.4 \cdot B^2) \cdot (T-4.2) \qquad (5.1)$$

Using quench analyses as described in the book by M. Wilson [11], peak temperatures and voltages generated during a quench were predicted to be within acceptable levels (Table 5.1). A worst case scenario was assumed, where the coil energy was dissipated within the coil.

Table 5.1: Coil and Wire Parameters for Racetrack Magnet

Coil Design		
Inner end radius (mm)	=	55.0
Outer end radius (mm)	=	95.0
Coil section ($\Delta y \cdot \Delta z$) (mm^2)	=	40.0x 38.0
Straight side length	=	221
Overall length (mm)	=	416
Projected fill factor(%)	=	> 80
Number of turns	=	647
Magnet strength at operating current (amp.-turns)	=	400,000
Design operating current (ampere)	=	618.24
Projected inductance (mH)	=	146
Stored energy at design current (kilojoules)	=	27.9
Peak Field at design current on ends (Tesla)	=	5.14
Peak Field at design current on straight sides (Tesla)	=	4.21
Projected peak quench temperature (K)	=	69.3
Projected peak voltage within winding(V)	=	900
Wire		
NbTi alloy	=	Nb 46.5wt%Ti
Cu:NbTi ratio	=	2:1
Wire size (bare nominal) (mm x mm)	=	2 x 1
Corner radius (mm)	=	0.33 - 0.38
Number of filaments	=	426
Insulation	=	Heavy Formvar
Guaranteed critical current (A) (at 4.2 K and 4 T magnetic field parallel to broad face of wire)	=	1480
RRR of copper stabiliser	=	> 150:1
Twist pitch	=	1 turn per 40 mm

5.2. Coil Frame Design

A racetrack coil frame similar to that described for the superconducting solenoid [4] is indicated in Fig. 5.2. The mean end radius of the winding was 75 mm, and the straight side lengths were 220 mm. Cooling channels were constructed to provide cooling (and support) in the case where the coil is mounted in a vacuum vessel. The first tests were planned of course with the coil and frame fully immersed, but later trials were planned where coolant would be present only in the indicated channels and the coil would be mounted in vacuum. The frame material was SS304L sheet of thickness 2mm.

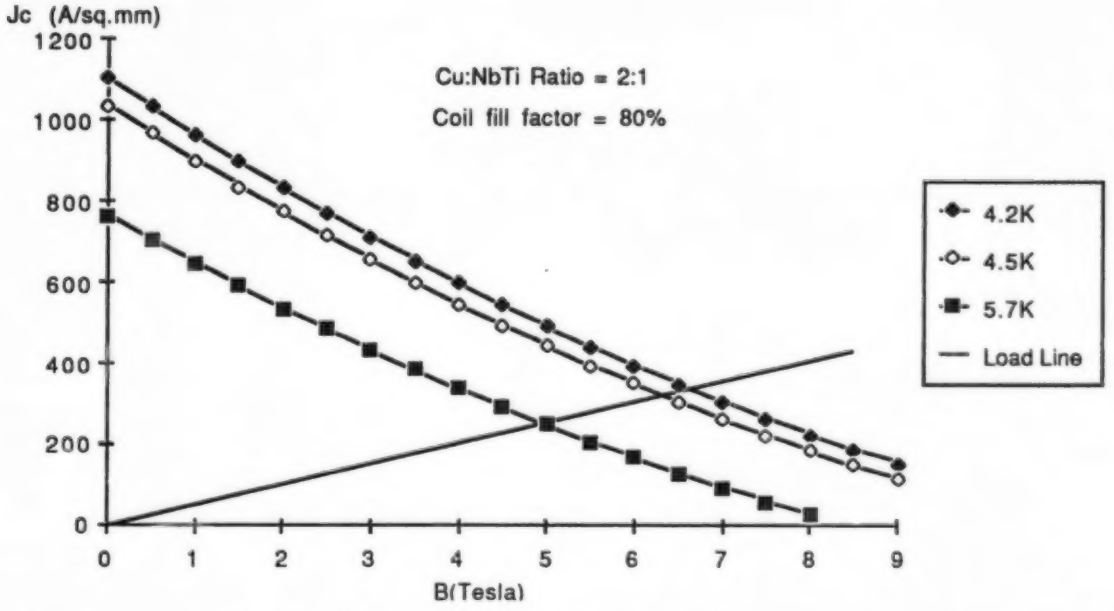

Fig. 5.1: **NbTi Jc vs field data [10], reduced by 2:1 Cu: NbTi ratio and coil fill factor of 80%, in relation to the coil load line for the peak field at the inner coil radius on the coil x axis (Fig. 4.5).**

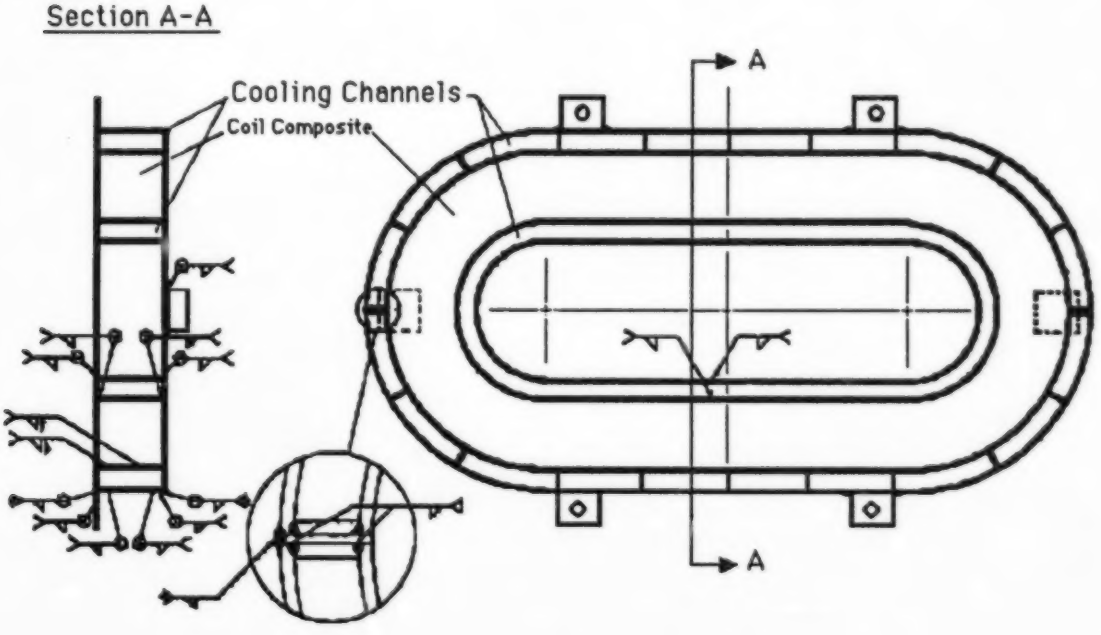

Fig. 5.2: **Ractrack coil winding and support frame from SS304L.**

5.3. Coil Winding and Impregnation

The winding of the coil was accomplished using a winding jig previously described [4]. The wire was loaded with a tension of about 8 lbs and a staggered winding pattern was used to improve winding and structural stability (Fig. 5.3). Subsequent layers of wire were displaced by half the wire width (≈ 1mm). Fibreglass cloth was placed between the layers of wire and also separating the outside of the winding and the SS304L winding channel. Special care was taken to reduce void volumes especially at the transition from one layer to the next.

After the winding was completed the wire entry and exit points from the frame were insulated and sealed, and the face plates welded in position. The winding cavity was then tested for leaks. The epoxy impregnation then followed with the coil mounted in a suitable oven and connected to a supply of premixed epoxy and hardener. The impregnation and curing parameters are listed in Table 5.2 for the Ciba-Geigy epoxy used. These are similar to the conditions described in reference 2.

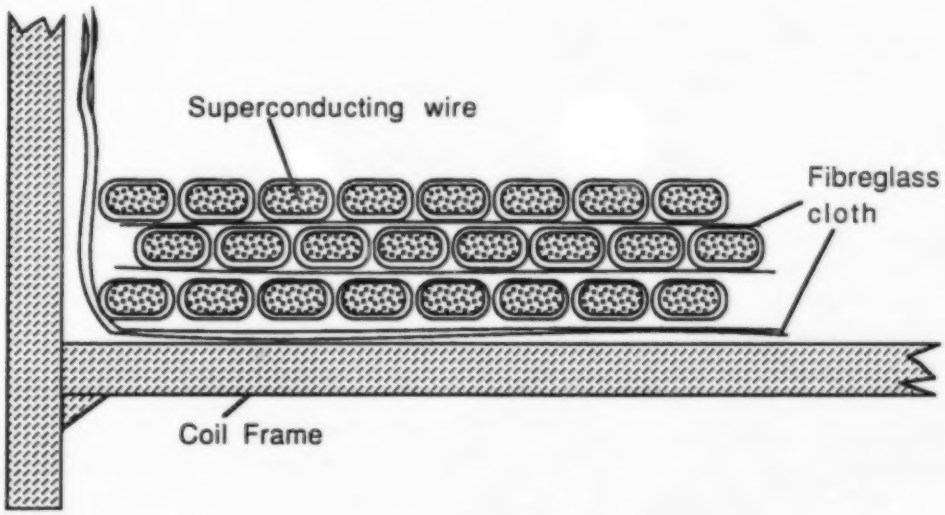

Fig. 5.3: **Winding pattern used for the racetrack coil.**

Table 5.2: Impregnation conditions for the racetrack coil winding.

Epoxy Resin	100 pbw Ciba-Geigy Resin 6010
Hardener	80 pbw type 906
Oven temperature during impregnation	85 C
Curing conditions	8 hours at 85 C 12 hours at 120 C

Once the coil had cooled to room temperature, the ends of the wires were attached to copper bus bars and checks made at room temperature of coil and joint resistance, insulation from the SS304 frame, coil inductance and general integrity. It was estimated that a fill factor of 82% was achieved with this winding. A view of the completed racetrack coil and frame is indicated in Fig. 5.4. The copper of the each bus bar was shunted by two Cu:NbTi wires of sectional area $2mm^2$.

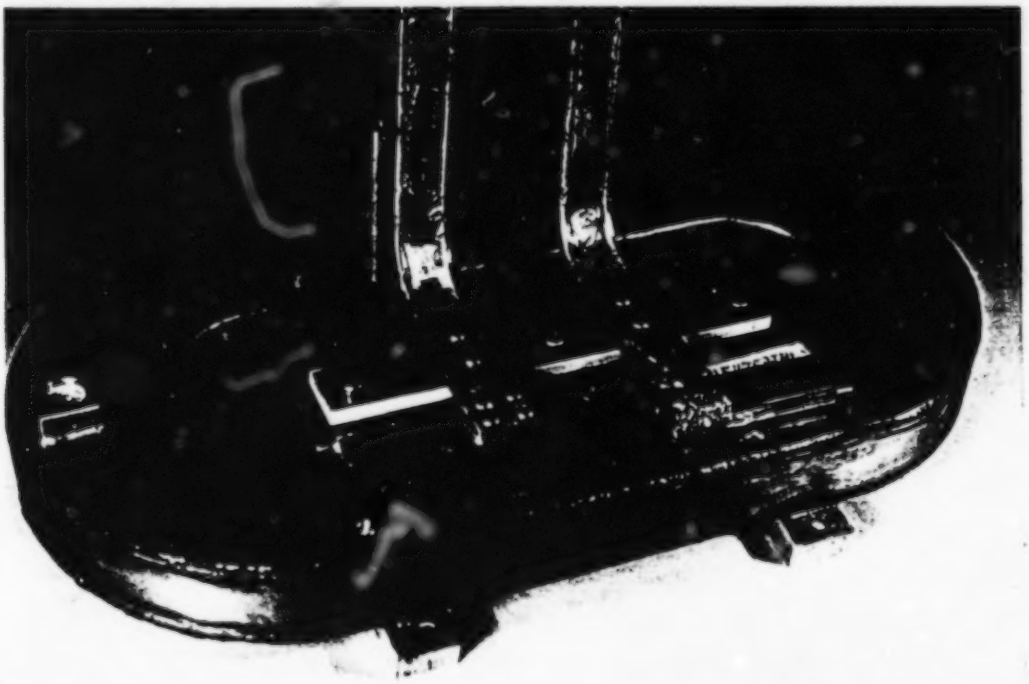

Fig. 5.4: **View of completed racetrack coil, SS304L frame and current lead bus bars**

5.4. Strain Gauge Instrumentation

Prior to testing of the racetrack coil performance, strain gauges were installed. It was decided to measure the displacement induced across the straight sides of the racetrack using the configuration outlined in Figs. 5.5 (a) and 5.5 (b). Two Karma alloy gauges (#WK-15-250BG-350) aligned to measure the transverse strain, were bonded to thin strips of brass foil (12.7 mm wide x 0.25 mm thick). These were the active gauges. The ends of the strips were clamped to two rectangular yokes mounted across the straight sides of the racetrack frame and the strips were tensioned by an adjustment mechanism. Brass foil was used to eliminate force effects due to material magnetic susceptibilty. The expected strain due to Lorentz loading was projected to be well within the strain level where the brass ceases to be elastic at 4.2 K (strain limit ≈ 1.5%). Identical dummy gauges were bonded on opposite sides of a brass block of geometry such that the active/dummy gauge pair separation was ≤1mm. The brass block was clamped to a G-10 mount which was not affected as the coil was energized.

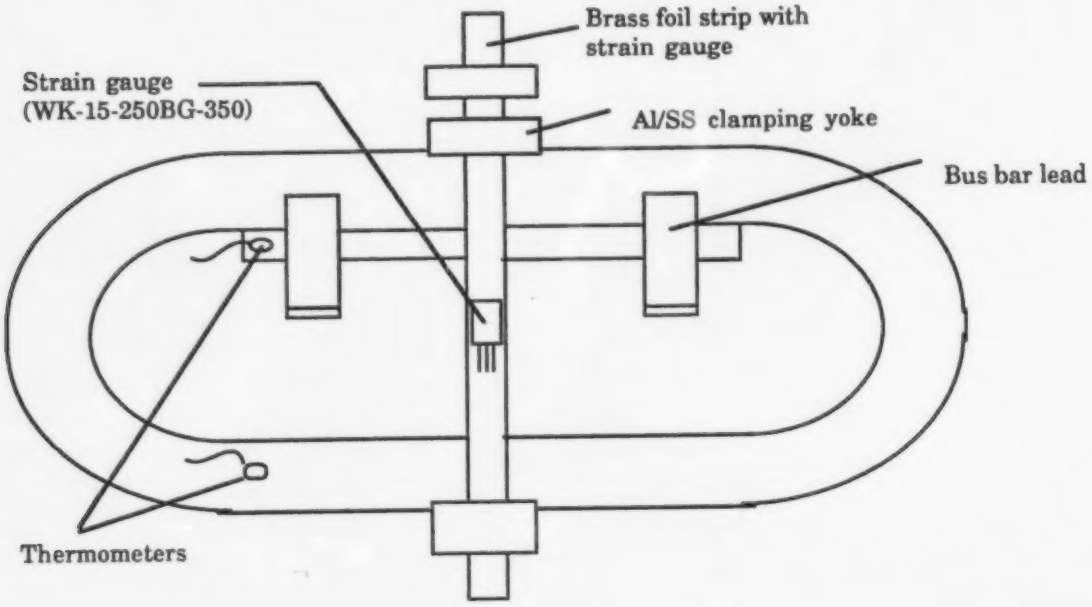

(a)

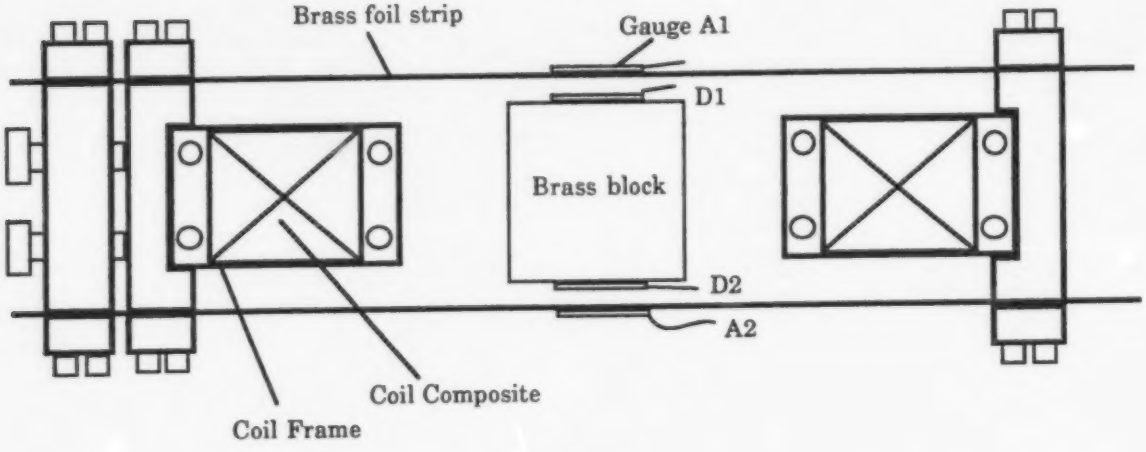

(b)

Fig. 5.4: **(a) Top view of strain gauge location for the racetrack coil measurements. (b) Side sectional view of locations of gauge pairs A1/D1, and A2/D2.**

5.5. Results of Liquid Helium Testing

The coil was mounted on an instrumented insert (He level indicator, thermometers, voltage and current leads etc) and tested at liquid helium temperatures with the coil and frame fully immersed (Fig. 5.5). The current in the coil was cycled slowly from zero up to the point where a quench occurred. At the same time, strain data were recorded from the gauge pairs (A1, D1), and (A2 , D2).

5.5.1. Training Performance

The coil training (critical current and critical current density) data are indicated for nine successive quenches in Figs. 5.6 (a), and 5.6 (b). The coil reached the design current after 3 training cycles and then apart from the 5th trial where the current was ramped too fast, remained above the design value of 618 amperes until it reached the short sample critical current at the 9th quench (I_{design} = (magnet strength/ no. of turns) = $4x10^5/ 647 = 618.24$ A). The peak current was estimated from the peak field calculation and the variation of Ic with field (Fig. 5.1). The racetrack coil behaviour was similar to that observed with a similarly prepared solenoid and it was concluded acceptable behaviour had been achieved.

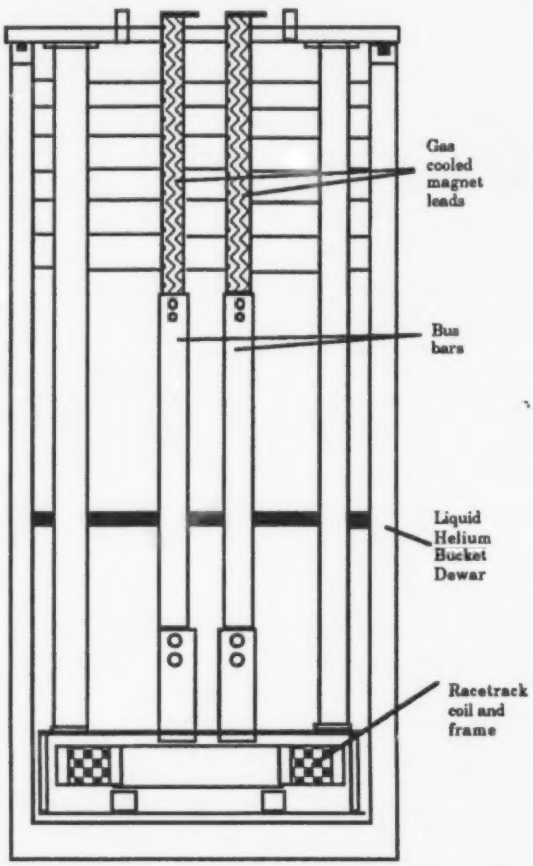

Fig. 5.5 : **Racetrack coil mounted in liquid helium test dewar.**

The critical current density Jc vs trial number is indicated in Fig. 5.6(b) where Jc is computed using an estimated coil sectional area of 40x38 = 1520 sq.mm.

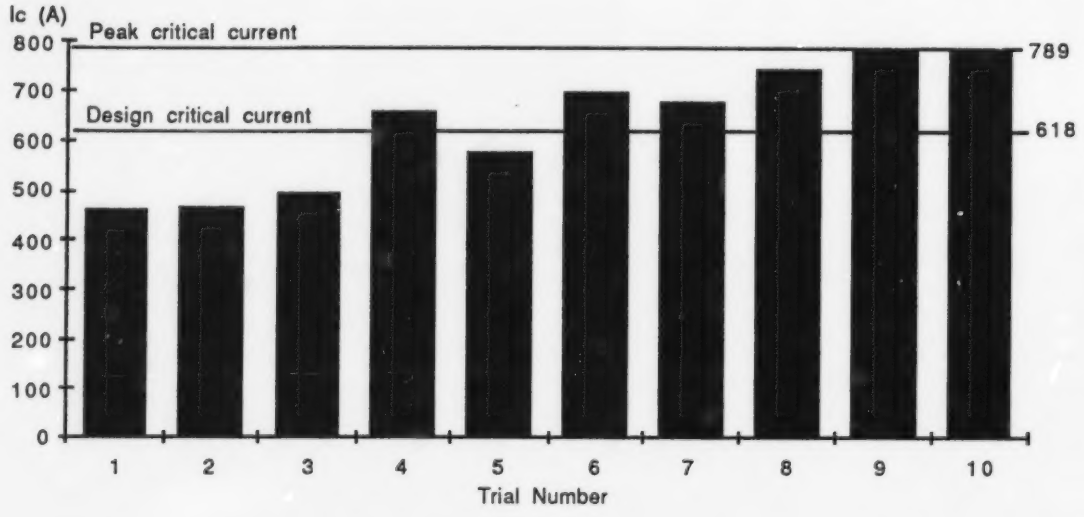

(a)

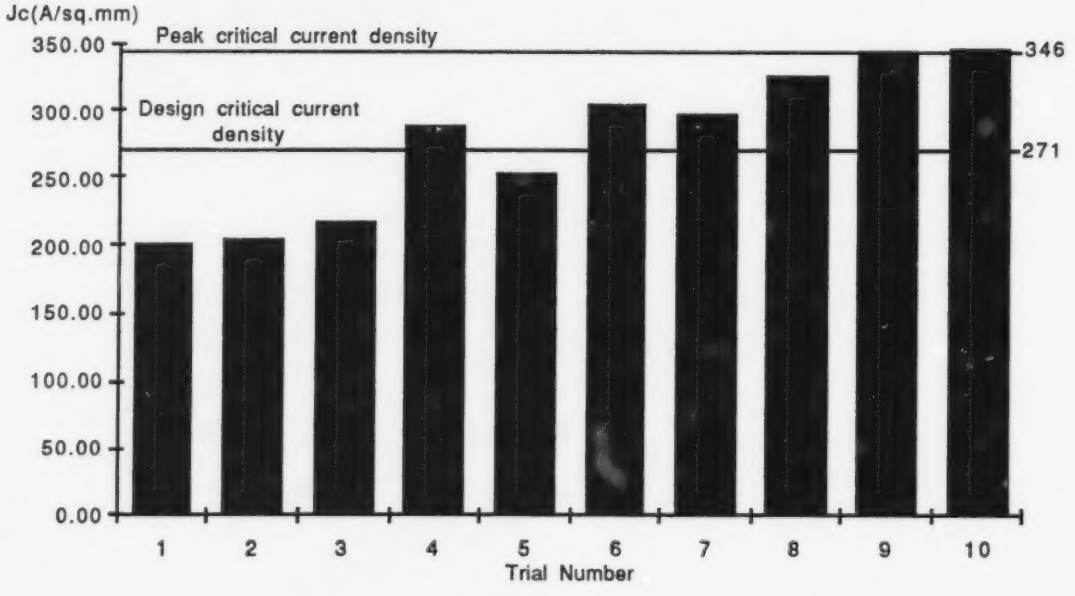

(b)

Fig. 5.6 : **(a) Critical current vs quench trial number.**
(b) Critical current density vs quench trial number.

5.5.2. Measurement and Interpretation of Transverse Strain

The normalized strains vs coil currents measured with the gauge pairs A1/D1, and A2/D2, whose locations are indicated in Fig. 5.4, are shown in Figs. 5.7(a) and 5.7(b) for quench trials 1, 4, 6, and 8. These data appear to be much more reproducible than the data for the solenoidal coil (see Figs. 3.3, 3.4), and do generally follow a strain proportional to the Lorentz force. In fact, included with the data in Figs 5.7(a) and 5.7(b) is an experimental fit of the form

$$\text{Strain } (\mu m/m) = 0.00675 * (\text{current (A)})^2 \qquad \{5.1\}$$

which was the same for both gauge pairs. Reasonably good agreement between this simple functional form and the experimentally measured strains indicates that both gauge pairs and the yoke clamping system were operating correctly.

The transverse Lorentz force per unit length on an element of sectional area dy·dz of the racetrack coil is given by :

$$dF(x,y,z) = J \cdot B_z(x,y,z) \cdot dy \cdot dz \qquad (N/m) \qquad \{5.2\}$$

where J is the overall coil current density (A/m^2) (= NI/A for coil strength NI and section A), and $B_z(x,y,z)$ is the z-component of the magnetic field at the element dy·dz. For the racetrack magnet under consideration, the magnetic fields within the winding were computed for a suitable mesh of points, and then the lateral force density components determined by integration with respect to the y and z coordinates over the winding dimensions (see Fig. 4.5 for coordinate notation).

Fig. 5.8 indicates the variation of the lateral load density components T_x, T_y and the total $T_r = \sqrt{(T_x^2 + T_y^2)}$ as a function of x. These data are similar to the single filament racetrack results of Ooi and Jain [12], but with force density magnitude more than twice as large due to the force density being approximately proportional to the inverse of the mean side separation (for two infinite filaments of separation d, each carrying a current I, the Lorentz force between them is $F_L = \mu_0 \cdot I^2/2\pi d$ where $\mu_0 = 4\pi \cdot 10^{-7}$).

An estimate of the expected strain was computed as follows. The coil was divided into two main regions: (a) the straight sides and (b) the curved ends. On the straight sides, the lateral force density indicated in Fig.5.8 causes the coil and frame to bend outward. The total lateral load on the sides also causes the end semicircles to deform. The displacement Δy at the centre of a straight beam with simply supported ends is given by [13]:

$$\Delta y = \frac{T_y \cdot (1/\cos(kL/2) - 0.125 \cdot (kL)^2 - 1)}{k^2 \cdot P} \qquad \{5.3\}$$

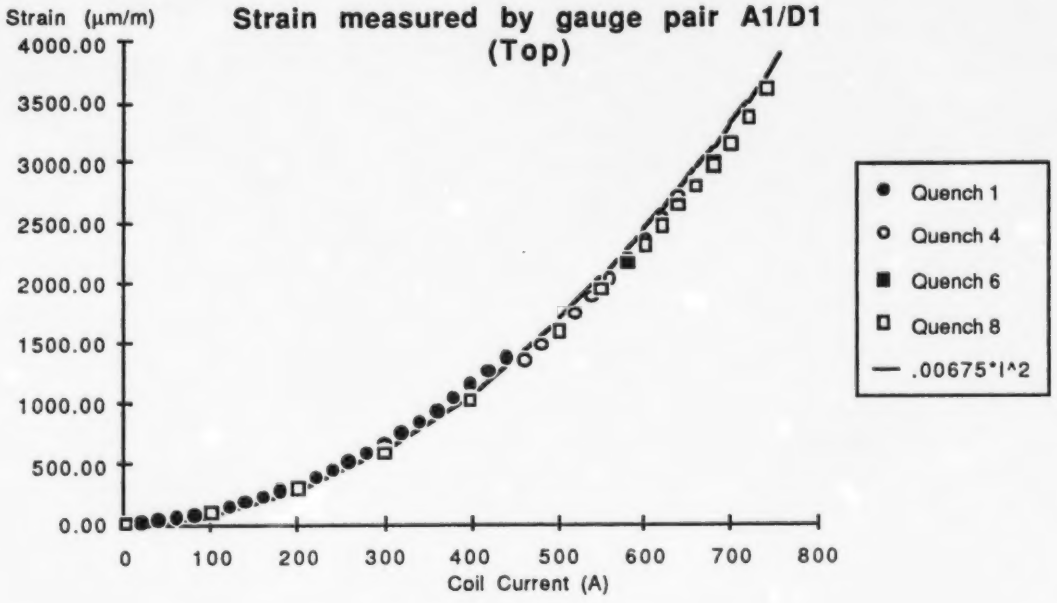

(a)

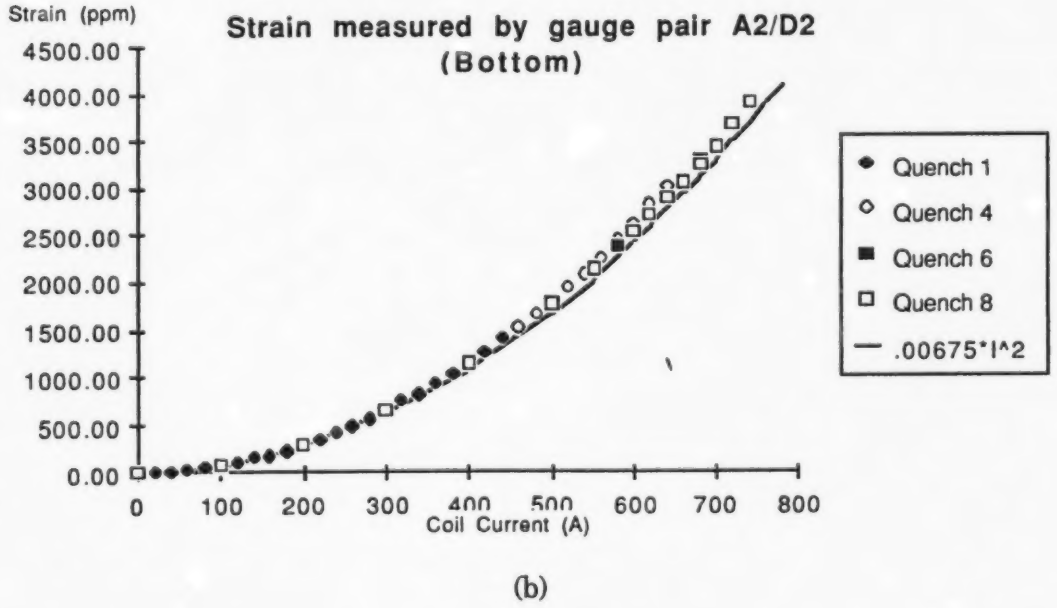

(b)

Fig. 5.7: **(a) Strain (μm/m) vs coil current for the gauge pair on the top brass strip (A1/D1).**
(b) Strain (μm/m) vs coil current for the gauge pair on the bottom brass strip (A2/D2).

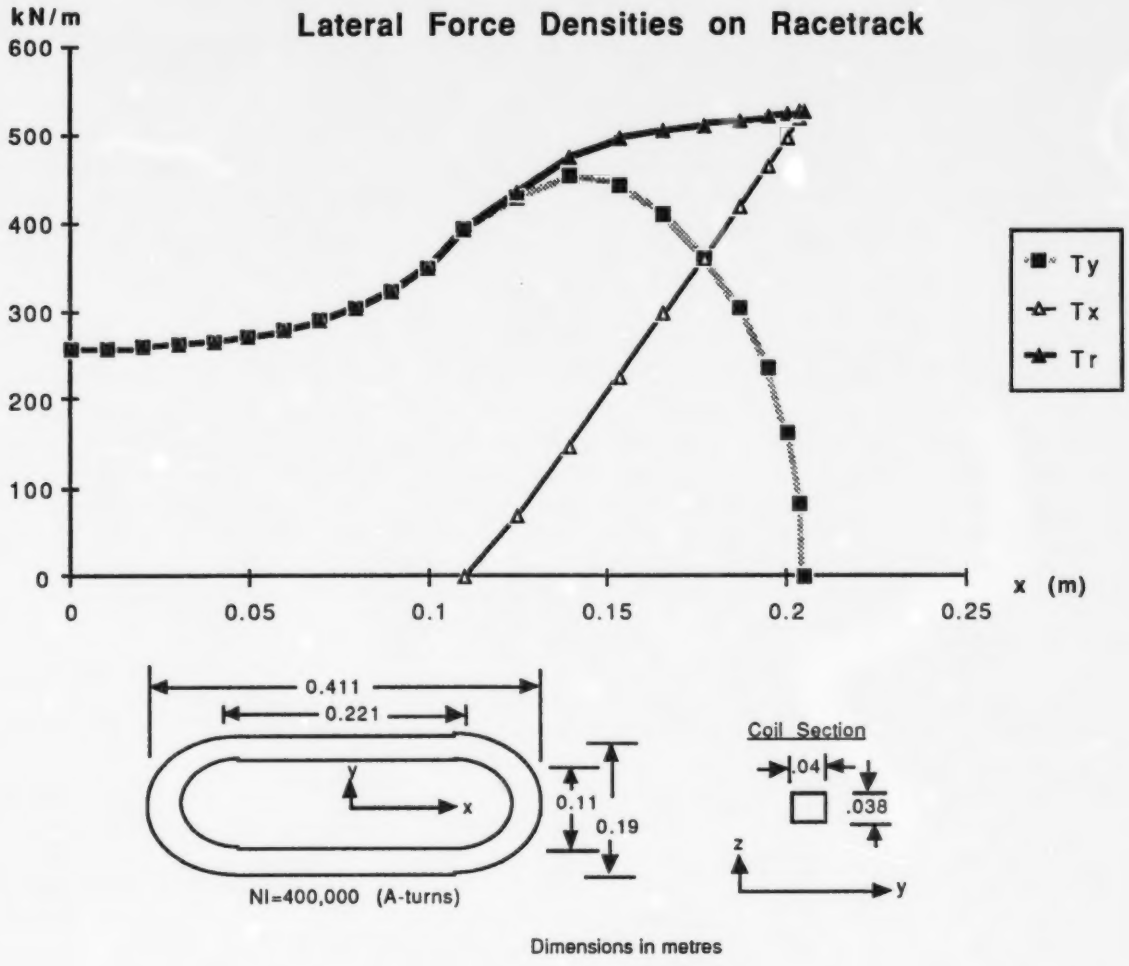

Fig. 5.8: **Lateral load density vs x for the racetrack parameters indicated**

where T_y = lateral load density; k = $\sqrt{(P/(E \cdot MI))}$
L = straight side length; P = load in x-direction
E = Young's modulus; MI = sectional modulus.

(Since T_y is directly proportional to I^2 , then $\Delta y \propto I^2$). The coil and frame have been treated as a composite beam, with sections shown in Fig. 5. 9. There are the two channels and the box round the coil, all of SS 304L, and the coil itself. The actual displacement at the centre of this composite beam was computed by the equal displacement method, where each section was taken to have the same displacement (Δy_i) caused by some fraction (T_i) of the total load density (T) given in Fig. 5.8. Thus all Δy_i are equal, and the T_i are subject to the condition $\Sigma T_i = T$. This allows a solution for the individual T_i and the displacement at the beam centre. For the straight sides, the result was: $\Delta y_{beam} = 7.6 \times 10^{-5}$ m for the

following set of parameters: NI= $4x10^5$, E_{ss} = $2.0x10^{11}$Pa, E_{coil}= $4.1x10^{10}$ Pa, P=26.13 kN, and T=375kN and the frame and coil parameters of the experimental coil (see Table 5.1). The load P was computed by integrating T_x over the 90^0 arc. The value of E_{coil} at 4.22K was taken from the paper by Weston [14] for a coil with a similar fill factor and Cu:NbTi ratio = 1.8:1.

For the semicircular ends, the deformation of a circular beam by a load T_y was used, where the beam was composite with the section indicated in Fig. 5.9. For a given part of the composite, the displacement was computed from

$$\Delta y = \frac{T_y \cdot R^3 \cdot (\pi k_1/4 - 2/\pi)}{E \cdot MI} \qquad (5.4)$$

where $k_1 \approx 1+2\beta$, and $\beta = MI/(A \cdot R^2)$ (5.5)

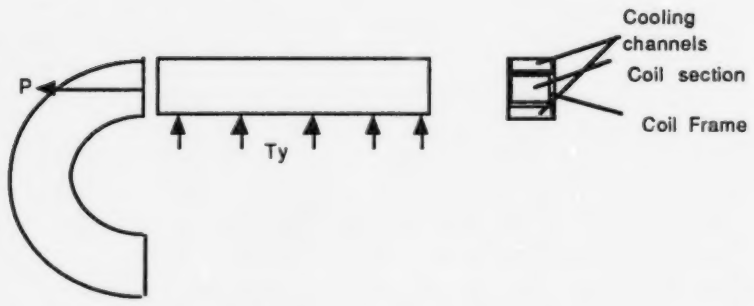

Fig. 5.9: **Model of coil and frame for strain estimation.**

Again the equal displacement method was used to compute the displacement resulting from bending the semicircular end. The result was Δy_{end} = $3.82x10^{-4}$m. Thus the displacement at the centre of the straight side is dominated by the bending of the semicircular ends of the racetrack. From this simplified model, the result for the total displacement of the straight side centre was Δy_{total} = $(3.82 +0.76)x10^{-4}$ =$4.58x10^{-4}$m, resulting in a strain for the experiment described of

$$(\Delta y/y)_{estimated} = (4.58x10^{-4}/0.11) = 4160\mu m/m \qquad (5.6)$$

(The strained lengths of the brass strips was 0.22m). This estimated strain is to be compared with the value of 2800-2900 μm/m as plotted in Figs. 5.7(a) and (b) for a current of 618 A in the coil corresponding to NI= $4x10^5$ A-turns. Considering the simplicity of the model, and the fact that the Young's modulus of the coil composite at 4.2 K was not accurately known, the agreement with the experiment is acceptable. It was concluded from these analyses that a reasonable understanding had been reached of the behaviour of the coil and frame at 4.2 K, while the coil was being energized.

6. PERSISTENT SWITCH

The contract required the acquisition of persistent switches for operation of the developed racetrack magnet in persistent mode. External vendors appeared willing to attempt to fabricate a high current switch (e.g. for currents up to ≈ 650 A and 1 T field) but were unwilling to guarantee stable operation much above 250 A. Accordingly, within the guidelines and general goals of the contract, it was decided to attempt to develop stable switches using CTF technology.

6.1. Persistent Switch Design

The superconducting magnets for a Maglev vehicle system are generally operated in persistent mode, in order to reduce cryogenic heat load and to remove the requirement for an on-board power supply for continuous energizing of the coils. This is accomplished by first charging the magnet up to some operational current level before the start of operational service, and then shunting the coil input terminals with a superconducting short (persistent current switch) which allows the current to flow for an extended period of time, with very small decay rate. The decay is caused by some loss in the coil-switch loop (usually joint resistances). The basic circuit is indicated in Fig. 6.1 where a superconducting coil of inductance L is shunted by a persistent switch of normal resistance R_{sw} , and also a protection resistance R_{prot} across the power supply terminals. The protection resistor is included in the circuit to protect the switch during the magnet quenching. The persistent current switch (PCS) is thermally operated, and has a built-in resistive heater for driving it into its normal state, where its resistance is R_{sw}.

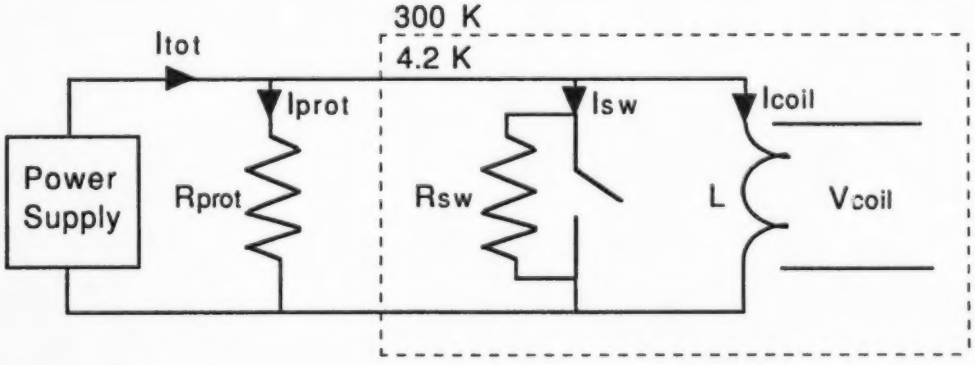

Fig. 6.1: **Circuit for Superonducting Coil and Persistent Switch**

A model of the behaviour of various PCS parameters as a function of time was established. This will now be briefly described. The voltage across the coil as a function of time is given by:

$$V_{coil}(t) = L\frac{dI_{coil}}{dt} \qquad (6.1)$$

The coil current is found by solving the following first order equation:

$$I_{tot}(t) = I_{coil}(t) + \frac{L}{R_{eq}} \cdot \frac{dI_{coil}(t)}{dt} \qquad \{6.2\}$$

where $I_{tot}(t)$ is the supply current at time t and R_{eq} is the parallel resistance:

$$R_{eq} = \frac{R_{prot} \cdot R_{sw}}{R_{prot} + R_{sw}} \qquad \{6.3\}$$

Two types of current ramp were considered :

(a) a linear ramp rate where $I_{tot}(t) = ß \cdot t$, with ß = constant, and

(b) an exponential ramp rate, $I_{tot}(t) = I_f \cdot (1 - \exp (\frac{-t}{T_s}))$ where I_f is the final current and T_s is a suitable time constant.

For a linear supply current ramp, the coil voltage and current are given by:

$$V_{coil}(t) = L \cdot ß \cdot [1-\exp(-\frac{R_{eq} \cdot t}{L})] \quad (0<t<t_1) \qquad \{6.4\}$$

$$I_{coil}(t) = ß \cdot [t - \frac{L}{R_{eq}} \cdot [1 - \exp(-\frac{R_{eq} \cdot t}{L})] \quad (0<t<t_1) \qquad \{6.5\}$$

The power dissipated in the switch during the energization of the coil is given by

$$P_{PCS}(t) = \frac{V_{coil}^2}{R_{sw}} = \frac{1}{R_{sw}} \cdot ß^2 \cdot L^2 \cdot (1- \exp (-\frac{R_{eq} \cdot t}{L}))^2 \qquad \{6.6\}$$

Thus P_{PCS} is minimised by having as large a value of R_{sw} as possible.

It is clear from equation {6.5}, that the coil current will lag the supply current, and thus what is done is to ramp the supply current up to some final value I_f, reached after a time t_1, and to hold it constant at this value until the coil current approaches very close to I_f , after a total time t_2 . Under these conditions during the time interval $0 < t < t_1$), I_{coil} and V_{coil} are given by equations 6.4 and 6.5. In the interval $t_1 < t < t_2$, the coil voltage and current are given by:

$$I_{coil}(t) = I_f - (I_f - I_{coil}(t_1)) \cdot \exp (- \frac{R_{eq} \cdot (t-t_1)}{L}) \qquad (t_1<t<t_2) \qquad \{6.7\}$$

$$V_{coil}(t) = V_{coil}(t_1) \cdot \exp (- \frac{R_{eq} \cdot (t-t_1)}{L}) \qquad (t_1<t<t_2) \qquad \{6.8\}$$

The total Joule heat dissipated in the PCS (Q_{PCS}) is computed by integrating equation 6.6 over the complete time interval $0 < t < t_2$. This is given by

$$Q_{PCS} = \frac{(\beta \cdot L)^2}{R_{sw}} \cdot [t_1 - \frac{2L}{R_{eq}} \cdot [1 - \exp(-\frac{R_{eq} \cdot t_1}{L})] + \frac{L}{2R_{eq}} \cdot [1 - \exp(-\frac{2R_{eq} \cdot t_1}{L})]]$$

$$+ \frac{V_{coil}(t_1)^2}{R_{sw}} \cdot \frac{L}{2R_{eq}} \cdot [1 - \exp(-\frac{2R_{eq} \cdot (t_2 - t_1)}{L})] \quad \{6.9\}$$

In the case of an exponential supply current ramp rate

$$I_{tot}(t) = I_f \cdot (1 - \exp(-\frac{t}{T_s})) \quad \{6.10\}$$

the coil voltage and current are given by:

$$V_{coil}(t) = \frac{LI_f}{\tau + T_s} \cdot (\exp(-\frac{t}{\tau}) - \exp(\frac{t}{T_s})) \quad \{6.11\}$$

$$I_{coil}(t) = I_f \cdot (1 - \frac{\tau \cdot \exp(-\frac{t}{\tau}) - T_s \cdot \exp(-\frac{t}{T_s})}{\tau - T_s}) \quad \{6.12\}$$

Here $\tau = L/R_{eq}$, and T_s is the time constant associated with the exponential current ramp.

In the above analysis, the switch resistance has been assumed to be time independent. However in the first switch constructed of the same 2:1 Cu:NbTi wire used for the superconducting coils, the copper stabiliser resistivity is temperature and field dependent and this affects the model. This dependency arises from the electrical magnetoresistance of the rather pure Cu stabiliser used in commercial wires. The resistivity of the stabiliser at temperature T in a field B may be written as :

$$\varrho(B,T) = \varrho(0,T)(1 + a_0 + a_1 \cdot \log_e(B \cdot \frac{\varrho(0,273)}{\varrho(0,T)}) + a_2 \cdot (\log_e(B \cdot \frac{\varrho(0,273)}{\varrho(0,T)}))^2) \quad \{6.13\}$$

where $a_0 = -7.008$, $a_1 = 1.383$, $a_2 = -0.0298$.

In the actual model used for the switch, the simulation was carried out by taking small steps in time (Δt) and determining the parameters at time t based on the parameters at $t-\Delta t$. Thus:

$$I_{coil}(t) = \frac{I_{tot}(t) + I_{coil}(t-\Delta t) \cdot \frac{L}{R_{eq}(t) \cdot \Delta t}}{1 + \frac{L}{R_{eq}(t) \cdot \Delta t}} \quad \{6.14\}$$

$$V_{coil}(t) = L\frac{I_{coil}(t) - I_{coil}(t-\Delta t)}{\Delta t} \quad (6.15)$$

$$R_{eq}(t) = \frac{R_{prot} \cdot R_{sw}(t)}{R_{prot} + R_{sw}(t)} \quad (6.16)$$

$R_{sw}(t)$ was computed using equation 6.13 for the specific coil geometries selected.

The currents in the switch and protection resistor were computed from

$$I_{sw}(t) = \frac{V_{coil}(t)}{R_{sw}(t-\Delta t)} \quad (6.17)$$

$$I_{prot}(t) = \frac{V_{coil}(t)}{R_{prot}} \quad (6.18)$$

The power dissipated in the switch due to resistive heating was computed from

$$P_{PCS}(t) = \frac{(V_{coil}(t))^2}{R_{sw}(t-\Delta t)} \quad (6.19)$$

and the helium boil-off rate derived from the power dissipation of equation 6.19 added to the built-in resistive heater power dissipation $P_{heater}(t)$.

In addition to the electrical model of the switch, a simplified thermal model was also developed based on the materials used. In actual construction, the switch wire and heater are insulated from the helium bath by a thickness of insulation (Fig. 6.2). In determining the switch temperature at time t (T(t)), the dominant heat flow from the switch was assumed to be along the switch wires.

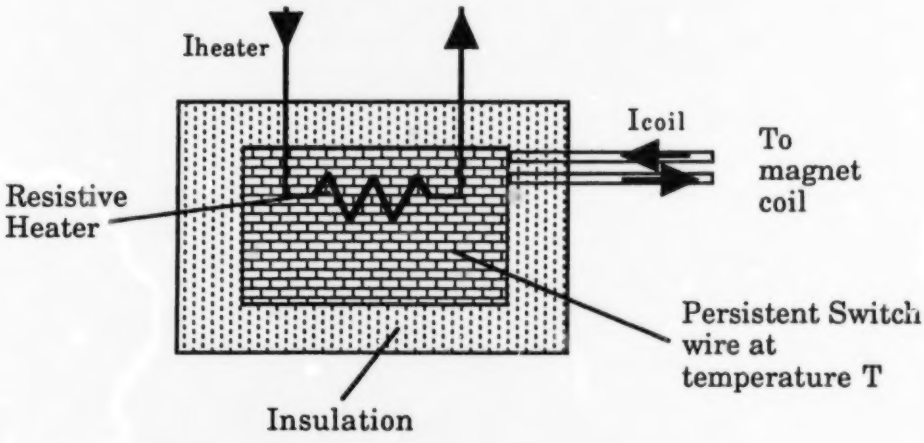

Fig. 6.2: **Persistent switch model**

The temperature of the switch wire inside the switch T(t), was determined from

$$T(t) = \frac{(P_{PCS}(t) + P_{heater}(t) - P_{cooling}(t))\cdot\Delta t}{m_1\cdot C_p(T(t-\Delta t))_{NbTi} + m_2\cdot C_p(T(t-\Delta t)_{stab})} + T(t-\Delta t) \qquad (6.20)$$

where the cooling rate of the switch wires was taken as due entirely to the heat flowing into the main mass of wires via the wires themselves:

$$P_{cooling}(t) = \frac{K\cdot A\cdot(T(t-\Delta t)-4.224)}{d} \qquad (6.21)$$

$C_p(T)$ are the specific heats of the NbTi of mass m_1 and the wire stabiliser material of mass m_2 (copper for switch #1 and CuNi for switch #2). A is the area of the conductor, K is an effective thermal conductivity and d is an effective length between the bath temperature (4.224 K) and the switch wire temperature T(t).

Various switch geometries were investigated and the time dependencies of various parameters of the circuit in Fig. 6.1 were determined. To present a flavour of the results of the simulation, the parameters of Table 6.1 for a switch PCS#1 will be presented in the next series of figures.

Table 6.1: Persistent Current Switch Simulation Parameters

Superconducting coil parameters	L(H)	=	0.146
	R_{prot}(Ohm)	=	0.05
Power Supply Parameters (exponential ramp)	T_s(sec)	=	465
PCS#1 Parameters			
Switch wire Cu:NbTi ratio		=	2:1
Wire length (m)		=	70
Field at PCS location (B/I (gauss/A))		=	10
RRR of Cu stabiliser		=	300
R_{sw}(B=0,T=10K) (ohm)		=	29.2×10^{-3}
Heater resistance (ohm)		=	188
Minimum heater power to drive PCS#1 normal(W)		=	1.0575

Figures 6.3(a) to 6.3(g) present the results of the simulation for the PCS#1. In Fig 6.3(a) the behaviour of I_{tot} and I_{coil} as a function of time are indicated where the supply current is ramped exponentially to a coil bias of 640 A. The coil voltage variation in time is indicated in Fig. 6.3(b) and the sharp peak projected in the time interval $0<t<100$ sec results from the rapid increase in the switch temperature caused by Joule heating power indicated in Fig. 6.3(d). The switch resistivity is controlled by the resistivity of copper stabiliser which changes with time as indicated in Fig. 6.3(f). As the temperature of the switch rises, the cooling power

also increases as indicated in Fig. 6.3(d) until equilibrium is reached in the range 100<t<375 sec when the peak supply current at 640 A is reached. This precipitates various exponential decays as indicated in Figs 6.3(b)-(d),(f)-(g). Final decays are caused by switching off the heater current at 470 sec. The total projected helium loss during coil energizing is indicated in Fig. 6.3(e).

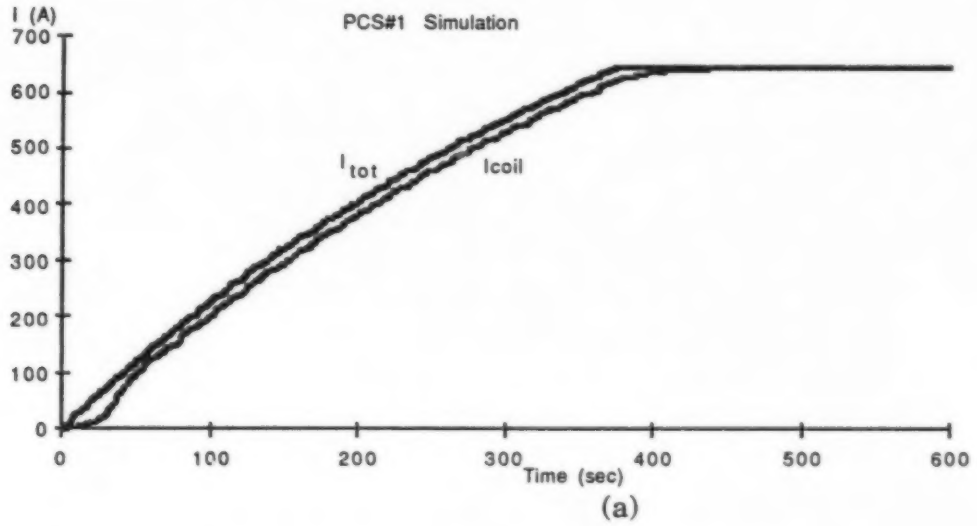

(a)

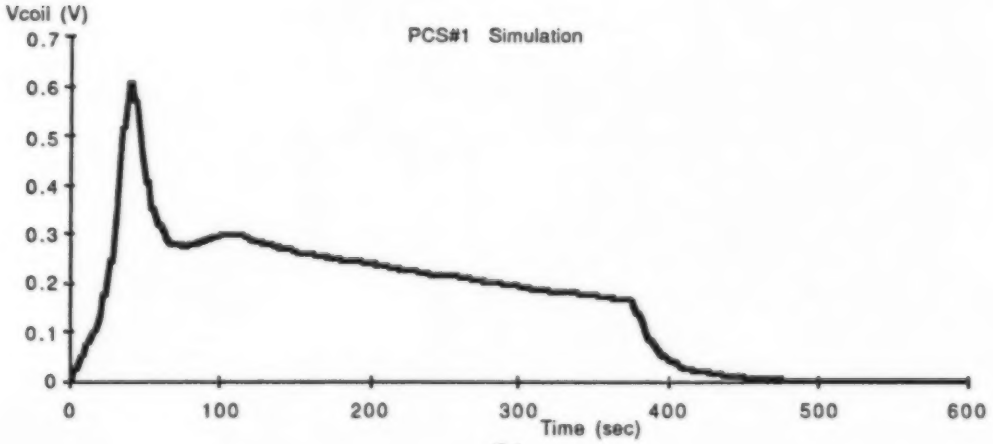

(b)

Fig. 6.3: **(a) Supply and superconducting coil voltage vs time. (b) Superconducting coil voltage vs time.**

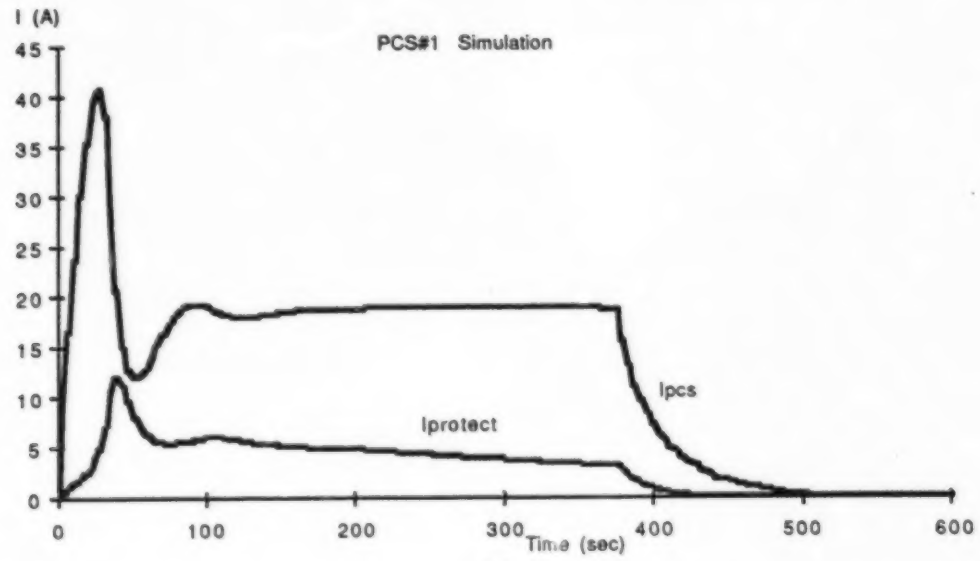

(c)

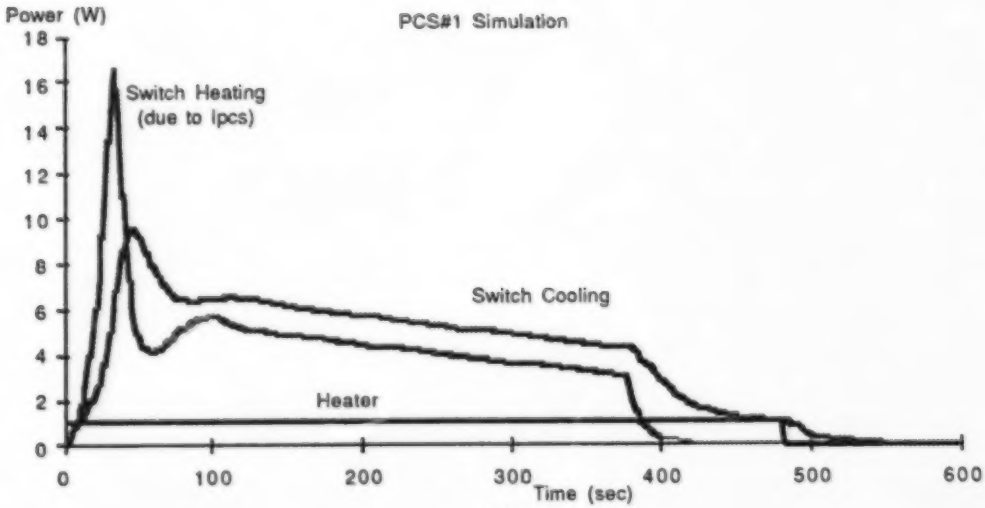

(d)

Fig. 6.3: (c) Current through PCS and protection resistor vs time.
(d) Power dissipation in switch and heater and cooling power of LHe bath on switch vs time.

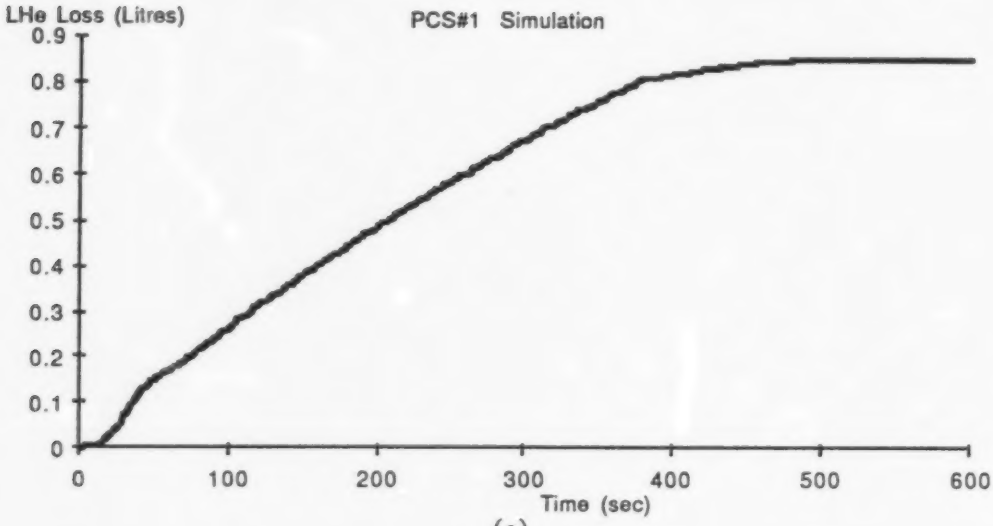

(e)

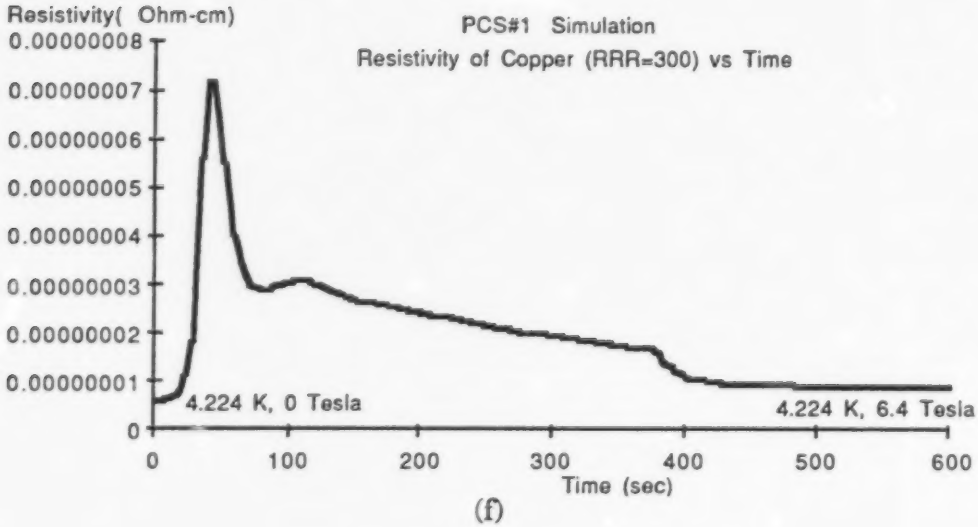

(f)

Fig. 6.3: **(e) Liquid helium loss during operation of switch vs time**
(f) Resistivity of sc wire copper stabiliser vs time

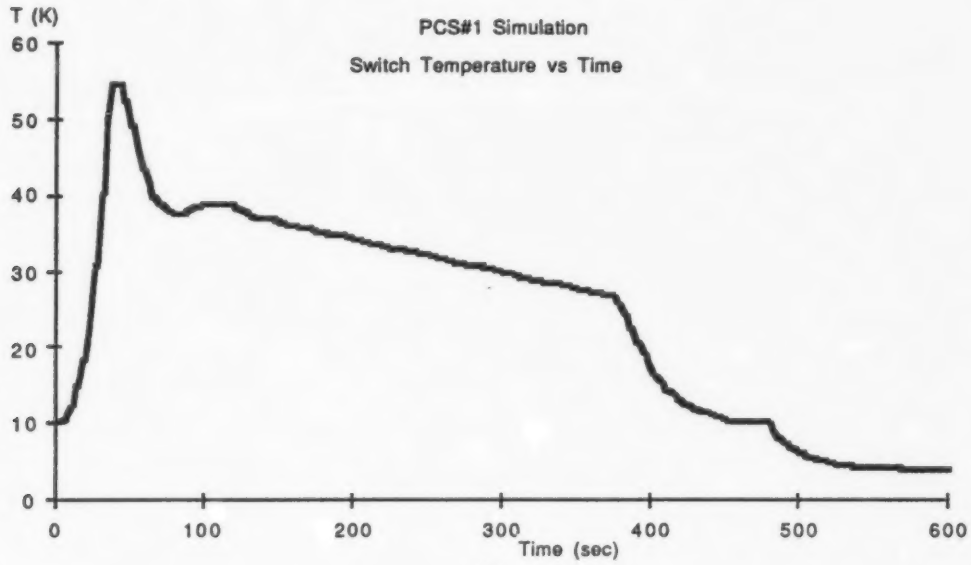

Fig. 6.3: **(g) Switch temperature vs time**

6.2. Fabrication of Persistent Switches

Two types of persistent switch have been fabricated, the first labelled PCS#1 was a low resistance type wound with 2:1 Cu:NbTi wire of nominal section 2mm x 1 mm. This switch behaviour was projected in Figs 6.3 (a)-(g). In order to reduce helium loss, commercial switch wire was acquired with Cupro -Nickel stabiliser in the ratio 1.5:1 CuNi:NbTi instead of the copper.

The switches were fabricated by winding the switch wire in bi-filar form to minimize the switch inductance. Also, at the same time, Nichrome heater wire was wound between the switch wire turns. The wires were wound on a cylindrical former and then sealed in. The winding layers were separated by fibreglass cloth. After sealing and leak testing the winding cavity, epoxy was introduced to mechanically stabilize the windings. After oven curing the epoxy, 2.54 cm wide x 0.6 cm thick copper bus bars were added for mechanical and electrical stability.

The principal parameters of the two switches are indicated in Table 6.2. Since the critical current for a single strand of the CuNi:NbTi wire was quoted at ≈ 330 A for a 1 Tesla field, 4 strands in parallel were used.

Table 6.2 Persistent Current Switch Parameters

	PCS#1	PCS#2
Switch Wire	2:1 Cu:NbTi	1.5:1 CuNi:NbTi
Bare size	2mm x 1mm	0.8 mm dia.
Insulation	Heavy Formvar	Heavy Formvar
Switch Wire Length	70 m, single strand	13.7 m x 4 strands in parallel
PCS dimensions (dia x height)	12 cm x 5.5	10 cm x 6.86 cm
No. of layers	28	4
Total No. of turns/layer	14	55
Switch Resistance (T=300K)	0.9 ohm	2.09 ohm
Switch Resistance (T= 11 K, B=0T))	0.0099 ohm	1.2 ohm
Design critical current at B=1 T	1200 A	1330 A
Heater Wire	Nichrome AWG#28	Nichrome AWG#28
Heater wire length	22.5 m	24.7 m
Heater resistance (300 K)	192 ohm	213 ohm
Heater resistance (off, T≈ 11 K)	188 ohm	209 ohm
Minimum heater current to drive switch normal	75 mA	55 mA
Time to drive switch normal	16 sec	32 sec

6.3. Tests of PCS#1 at Liquid Helium Temperature

PCS #1 was tested at 4.224 K with the switch mounted and instrumented in a large test dewar at the end of bus bar current leads (see Fig. 5.5). With this configuration in zero field, the switch did not quench for currents up to 950 A. After PCS#1 was connected across the terminals of the racetrack coil in LHe, the voltage appearing across the switch as a function of time after the heater was turned on ($V_{coil}(t)$) is indicated in Fig. 6.4. The general form and magnitude of the $V_{coil}(t)$ vs t curve was reproduced in the experiment ($V_{PCS}(t)$ in this case), indicating reasonable agreement with the model. The initial voltage spike was not reproduced in practice, no doubt because of the simplified model of the thermal response for a relatively complex geometry. The thermal behaviour of the PCS is quite difficult to model due to the lack of accurate knowledge of thermal parameters such as thermal conductivities and heat capacities of the various constructional materials as a function of temperature.

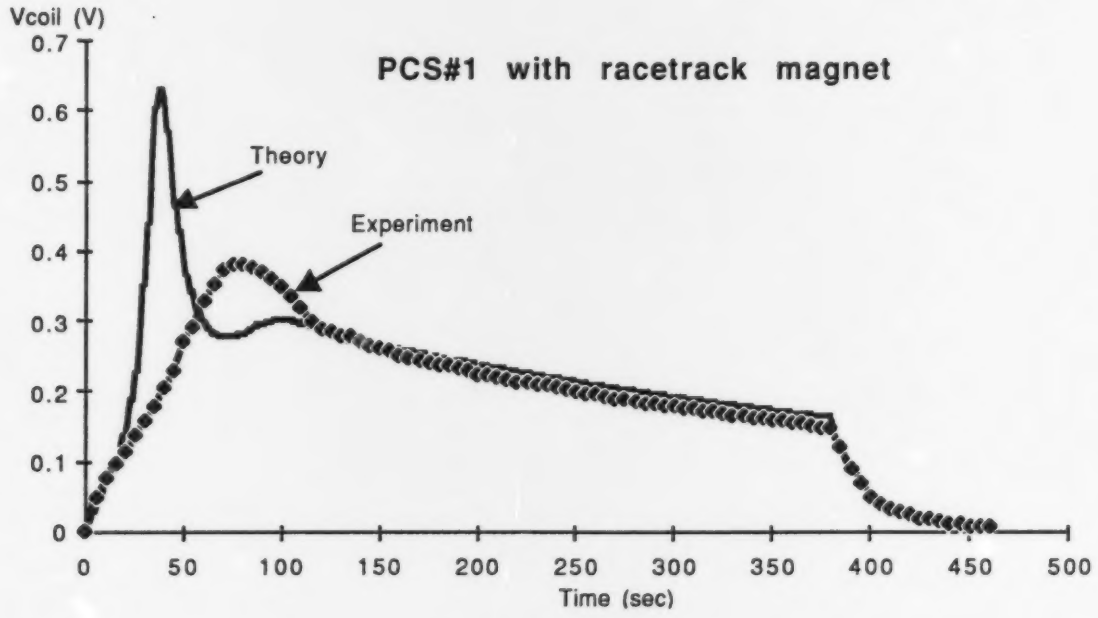

Fig. 6.4: **Comparison of theory and experiment for PCS#1 with the racetrack coil.**

6.4. Operation of Superconducting Coils in Persistent Mode

Several experiments were carried out to test the operation of the two switches PCS#1, and PCS#2, in persistent mode with the epoxy impregnated superconducting coils which have been fabricated during this and the previous contract. The arrangements were as follows:

(a) Racetrack magnet + PCS#1
(b) Solenoid magnet + PCS#2

where the switches were mounted across the current supply bus bars as schematically indicated in Fig. 6.5. Views of the two physical configurations are indicated in Figs. 6.6 and 6.7 for PCS#1 with the racetrack coil and PCS#2 with the solenoidal coil. Particular care was taken to ensure that very low contact resistances were present in the coil-switch circuit. Thermometers were mounted on the switch and the superconducting coil and the helium level was separately monitored with a superconducting wire level indicator. To measure the decay in the coil current while in persistent mode, a Hall probe magnetometer was used to measure the magnetic field vector at a specific distance R from the coil centre (Fig. 6.5),and then the current computed using the software described in section 4.

The experiments were conducted as follows with the coils and switches at 4.224K:

- With the switch open ($R_{sw} > 0$), energize the coil.
- After the operating current is reached, switch off the heater current.
- Wait until $R_{sw} = 0$, usually < 1 minute.
- Quickly ramp down the power supply current to zero.
- Observe the decay of the coil field with time using the magnetometer located near the dewar.

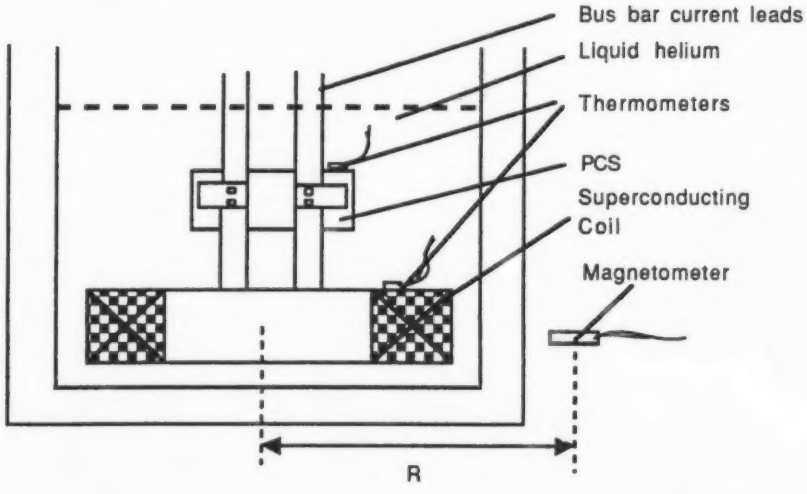

Fig. 6.5: **Arrangement of superconducting coil and PCS.**

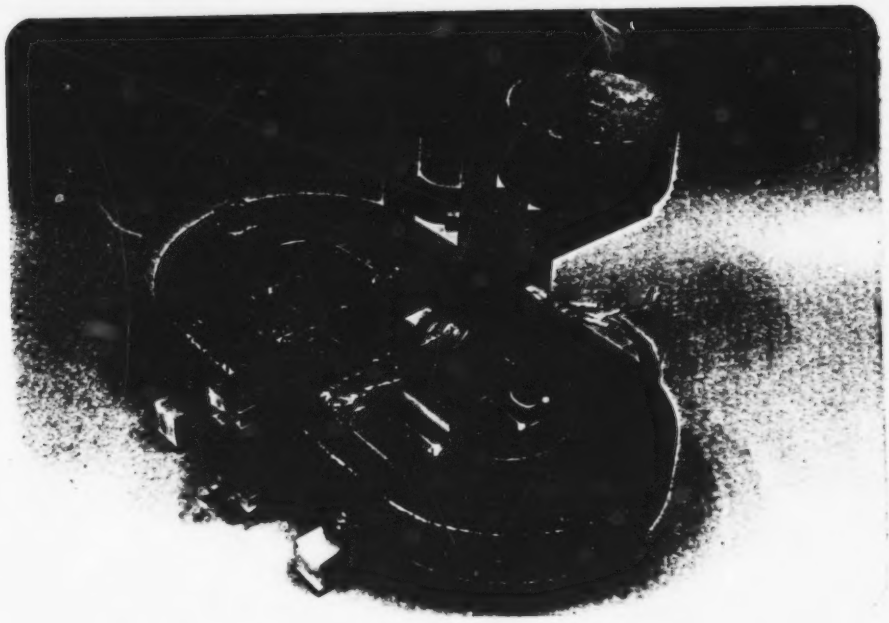

Fig. 6.6: **View of physical arrangement of racetrack coil and frame and PCS#1.** The switch location was selected based on a peak field at the switch of 1 T.

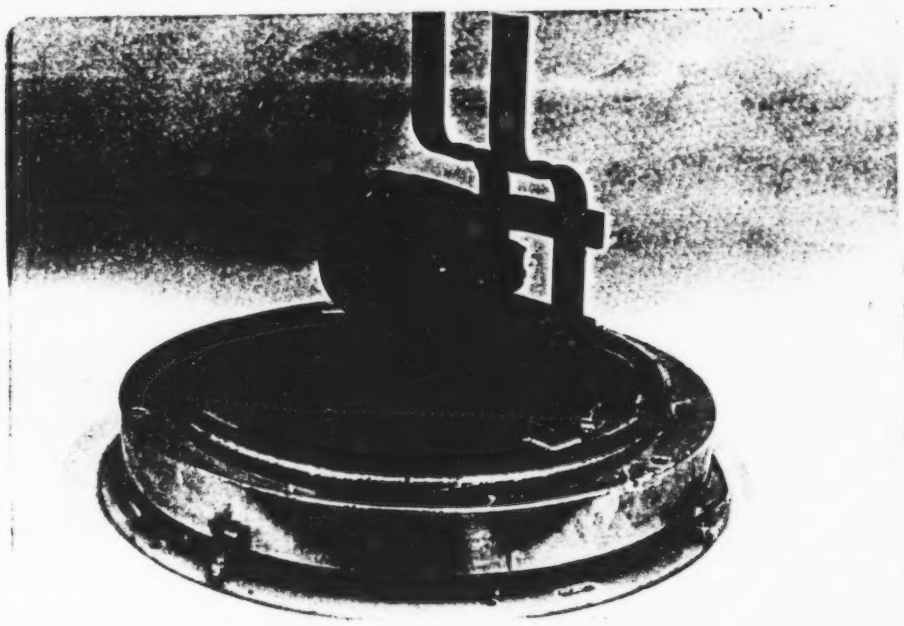

Fig. 6.7: **View of physical arrangement of solenoidal coil and frame and PCS#2.** The switch location was selected based on a peak field at the switch of 1 T.

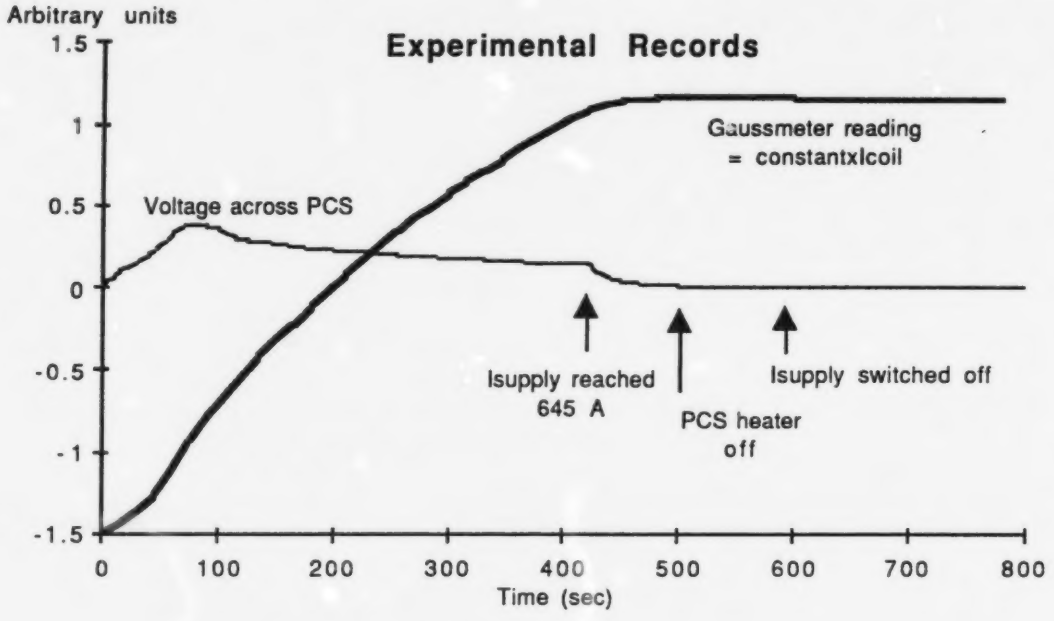

Fig. 6.8: **Experimental record of Hall probe magnetometer (coil supply current) and $V_{coil}(t)$ for the racetrack magnet and PCS#1 for starting current = 645 A.**

A portion of the data taken with the low resistance PCS#1 and the racetrack coil, is indicated in Fig. 6.8, with the starting current at 645 A. The decay was observed for 7.83 hours, resulting in a drop in measured field of 3.9%. The magnetic field B(t) (and current) are expected to decay according to $B(t) = B(0)\cdot\exp(-R\cdot t/L) = B(0)\cdot\exp(-t/\tau)$ and thus for PCS#1, one has

$$\tau_{PCS\#1} = L/R = \frac{-t}{\ln\left(\frac{B(t)}{B(0)}\right)} = -7.83/\ln(.96067) = 195 \text{ hours} \qquad (6.22)$$

With L = 0.146 H, $R = 2.1 \times 10^{-7}$ ohm.

Similar experiments were repeated with the PCS#2 and the solenoidal coil. The PCS#2 was superconducting for current flow up to 950 A in zero field. However, when connected across the solenoidal coil terminals the switch quenched after a time which depended on the current magnitude. Although this high resistance switch operated correctly for up to 10 minutes at 750 A, there were instabilities and the switch quenched causing rapid decay of the coil energy through the protection resistor. The switch quench was deduced from the fact that

only a small quantity of liquid helium was boiled off after the instability had taken place. Had the main solenoidal coil quenched, then considerably more helium cold gas would have evolved from the dewar.

The coil bias current was gradually reduced while checking for stability of operation in persistent mode. Stable persistence was observed for operating currents in the range 450-475 A with PCS#2. It is not clear whether the instabilities were related to intrinsic wire behaviour, imperfect switch construction, or local heating at joints etc. It was felt from the experiments conducted on this one high resistance switch that most of the decay resistance was due to copper at the joint. Also, this PCS#2 had a relatively poor epoxy impregnation cycle during fabrication, which could have seriously affected its mechanical integrity in the varying magnetic fields up to 1 T, to which it was subjected.

It is suggested that the number of CuNi:NbTi wires in parallel could be doubled (at the same time doubling the length per strand to 27.4 m without greatly increasing the switch volume and thus providing an increased margin of stability. Such a switch was planned, but experiments in this direction were halted to accomplish the amended work statement.

The data for the PCS#1 and PCS#2 switches are summarized in Table 6.3. The experiments with the prototype switches have indicated the following:

• It is possible to fabricate and operate epoxy impregnated coils in persistent mode to high current using PCS's with relatively low joint resistance and thus relatively long time constants.

• The low resistance PCS#1 fabricated using Cu:NbTi wire of size 2mm x 1mm worked well in fields up to 1 T and currents up to 645 A. Persistent mode experiments at higher currents were not attempted, but the switch appeared to operate in low fields at currents in excess of 900 A. This switch and loop resistance would be suitable for operation of a prototype levitation coil of the Canadian design (ref [3] Figs. 3.7 and 3.8).

• The high resistance PCS#2 worked well for currents up to 450 A. The instabilities at the higher operating current levels require further investigation.

Table 6.3 Summary of Persistent Mode Tests

Coil	Switch	R_{sw} (ohm)	L(H)	Time Constant (hours)	R(ohm)
Racetrack	PCS#1	0.099	0.146	195	2.1×10^{-7}
Solenoid	PCS#2	1.20	0.160	173	2.6×10^{-7}

7. CONCLUSIONS

From the results of this amended contract on development and testing of epoxy impregnated superconducting magnets of racetrack geometry, the following conclusions can be drawn:

1. The previously developed fabrication technology for epoxy impregnated superconducting coils was successfully extended to include racetrack configurations. A racetrack coil and frame design were implemented and tests indicated almost identical training behaviour to that previously observed with a superconducting solenoid. Operation to within a few % of the superconducting wire short sample critical current was achieved after a few training cycles with the racetrack coil immersed in liquid helium, thus vindicating the design. The coil operation reached the design current after the third quench and the short sample estimate after the eighth. The peak field in the windings at the short sample current value was estimated to be 6.8T.

2. Methods of making strain measurements at room to cryogenic temperatures (300K-4.2 K) were developed, and applied to both the superconducting solenoid and the racetrack magnets. The data from the solenoid tests where the strain gauges were attached to the outside of the SS304L support frame, indicated that the coil frame was probably slipping relative to the impregnated winding. The data from the racetrack coil and frame tests were significantly better than with the solenoid magnet, and a strain proportional to the square of the coil current was observed for operating currents I in the range $0 < I < \approx 800$ A. A simplified model of the composite coil plus frame system, was shown to provide a reasonable agreement with the observed strain across the sides of the racetrack magnet. It is useful to point out that the estimated lateral load density on the straight sides of the present racetrack coil is significantly higher than the estimated lateral load density on the sides of the full scale racetrack (1.06m long x 0.3 m width). The straight sides of the present racetrack are much closer together and as a consequence, the fields within the windings are much higher. Lateral strains of up to 0.4 % were tolerated by the present racetrack coil and SS304L frame at the peak operating current (789A), without noticeable damage or degradation of performance. As a safety feature in larger racetrack coil designs, the lateral strain can be limited to a suitable choice by welding transverse braces across the straight sides.

With these positive results, it is suggested that the coil weight could be reduced somewhat by reducing the Cu:NbTi ratio below the 2:1 ratio selected (e.g. toward 1:1), recognizing of course that the intrinsic stability of such windings would be reduced. The system is sufficiently complex however that the answer to this question should be experimentally verified.

3. During the contract, two types of thermally operated persistent current switches were designed, fabricated and tested alone, and also in operation with the two superconducting magnets, while immersed in liquid helium. A low resistance switch ($R_{sw} \approx 0.01$ ohm at 4.22 K) was connected across the terminals of the racetrack magnet, and operated successfully in persistent mode at 640 A. The total loop resistance estimated from the persistent current decay was $\approx 2 \times 10^{-7}$ ohm,

which is an acceptable value for operation of the superconducting magnets of the Canadian Maglev vehicle. It is felt that this joint resistance could be further lowered by suitable re-design. The second, high resistance switch ($R_{sw} \approx 1.2$ ohm at 4.22 K) operated successfully with the solenoidal magnet for currents up to ≈ 450 A, but displayed quench instabilities for currents above this value. The reasons for the instabilities were not clear, and further work with high resistance persistent switches is required for stable operation at higher operating currents.

The major results of this contract have thus advanced the state of the art of superconducting magnet technology within the Canadian context. Although the specific goals of the hardware development have been directed toward the EDS Maglev system option, the magnet fabrication methods have much wider applicability, essentially to any of the present-day small to medium size superconducting magnet applications.

REFERENCES

1. See e.g. N.E. Rudback, W.F. Hayes, A.A. Fife, A.R. Eastham, M. Audette, An Overview of Canadian Research and Development. Proceedings of the International Conference on Maglev Transport '85, pp13-20,Tokyo, Japan,1985, and references 1-4 cited therein. Publ by the IEEJ.

2. A. A. Fife, An Exploratory Study into Recooling Alternatives for Isochoric Dewar Operation. Transport Canada Report No. TP #2536, July, 1980.

3. A. A. Fife, H.J. Ensing, W. Westera, Design Study of a Lightweight Helium Cooled Superconducting Magnet. CTF Systems Inc. Report #RP-165-0184, January, 1984.

4. A.A. Fife, Fabrication and Testing of Reduced Scale Superconducting Magnets. Transport Canada Report No. TP7949E, July, 1986.

5. J.G. Bednorz, K.A. Muller, Zeitschrift fur Physik, B64, 189, 1986. M.K. Wu et al. Phys. Rev. Lett. 58, 908, 1987.

6. L.L. Sparks, Temperature, Strain and Magnetic Field Measurements in "Materials at Low Temperatures" Edited by R.R. Read, A.F. Clark . Published by American Society of Metals , Metals Park, Ohio 44073 (1983).

7. P.J. Walstrom, Strain Gauges for Superconducting Magnet Testing, Cryogenics, 20, 509,1980.

8. V. Arp, Stresses in Superconducting Solenoids, J. Appl. Phys. 48, 2026, 1977.

9. P.J. Hart, Universal Tables for Magnetic Fields of Filamentary and Distributed Circular Currents. Publ. by American Elsevier Publishing Co., 1967.

10. C.R. Spencer, P.A. Sanger, M. Young, The Temperature and Magnetic Field Dependence of Superconducting Critical Current Densities of Multifilamentary Nb_3Sn and NbTi composite Wires, IEEE Trans. Magn. 15, 76, 1979.

11. M. Wilson, Superconducting Magnets. Chapter 9. Publ. by Clarendon Press, Oxford, 1983.

12 B.T. Ooi, O.P. Jain, Analysis of the Moments and the Force Densities of the Superconducting Magnetic Levitation System for High Speed Guided Ground Transport. Transport Canada Report No. TP 1725, Aug. 1978.

13 R. J. Roark, W.C. Young, Formulas for Stress and Strain, 5th Edition ,1975. Tables 10 and 17.

14. W.F. Weston, Low Temperature Elastic Constants of a Superconducting Coil Composite , J. Appl. Phys. 46, 4458, 1975.